SELENIDE ISOTOPE GENERATOR

for the

GALILEO MISSION

[redacted]

MASTER

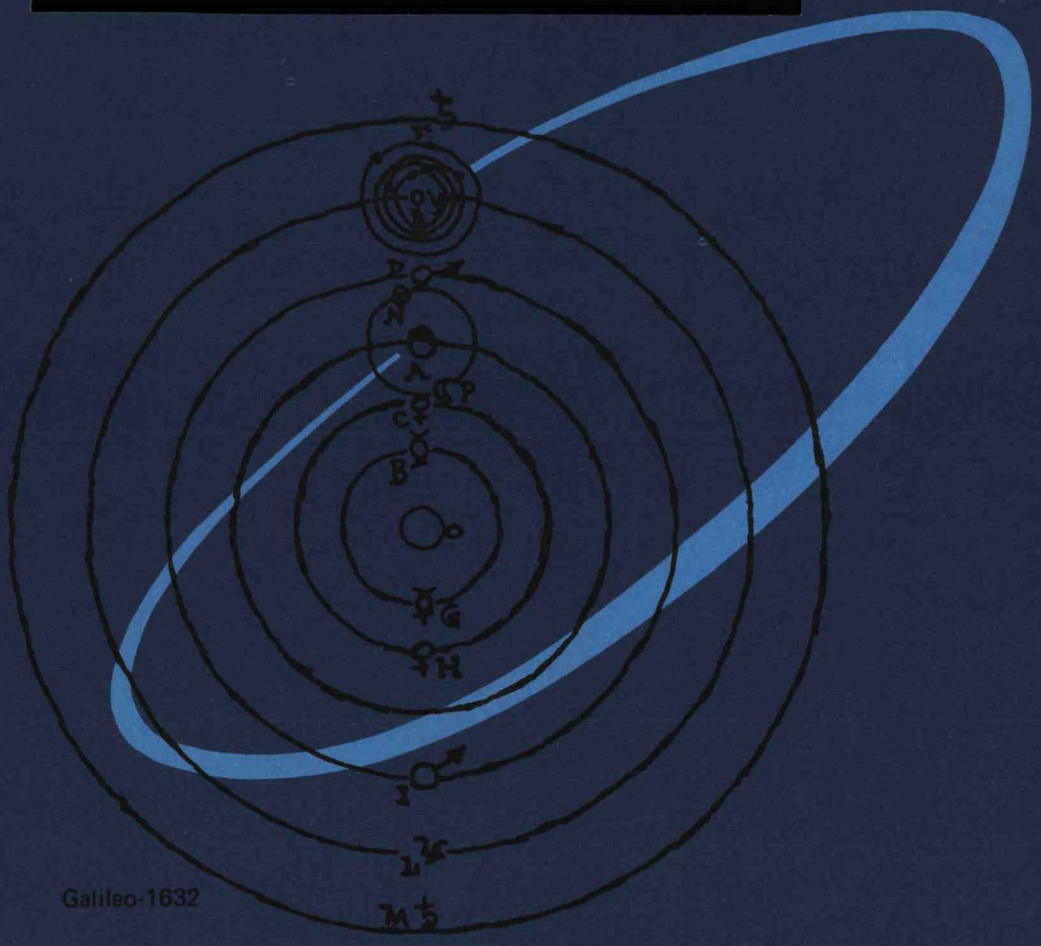

TELEDYNE ENERGY SYSTEMS

DISCLAIMER

Pictured on the cover is Galileo's drawing of the solar system, which includes the four satellites of Jupiter he discovered in the 1600's. A Renaissance professor, inventor and astronomer, Galileo perfected the telescope with which he made his Jupiter discoveries. The 1982 NASA mission to Jupiter is named in his honor. Like Galileo and his telescope, the NASA mission to the far reaches of outer space will be contributing to Mankind's never ending quest for knowledge.

SELENIDE ISOTOPE GENERATOR

for the

GALILEO MISSION

SIG THERMAL INSULATION EVALUATION TESTS

TES-33009-50

June 1979

W.E. Osmeyer
Program Manager

Prepared for the U.S. Department of Energy under Contract Number DE-AC01-78ET33009.

TELEDYNE ENERGY SYSTEMS
110 W. TIMONIUM RD., TIMONIUM, MD. 21093
PHONE: 301-252-8220 TELEX: 8-7780 CABLE: TELISES

EB

NOTICE

TABLE OF CONTENTS

LIST OF FIGURES

LIST OF TABLES

SIG THERMAL INSULATION EVALUATION TESTS

1.0 INTRODUCTION

Since the SIG program required the use of very high performance thermal insulation materials in rather severe thermal and environmental conditions, a thorough screening and testing program was essential.

The basic requirements imposed upon the systems were the ability to operate for 60,000 hours in a 1000°/150°C gradient with very high and essentially unchanging thermal efficiency. At the start of the program the actual environmental constitution was not completely defined. Therefore the various materials had to be evaluated for use in vacuum, xenon, argon, and helium atmospheres. Further, some of the insulation materials were required to exhibit reasonable load bearing ability (to support the heat source) while others were to be used in an essentially free standing mode.

Several types of materials were included in our preliminary survey. Most promising were oxide and carbonaceous fibrous insulations, oxide and carbonaceous foamed materials, and multilayer materials with both powder and cloth spacers. The latter were only viable for the vacuum option. In all, over one hundred materials from more than sixty manufacturers were evaluated from literature and manufacturers' data.

This list was pared to eighteen candidates in seven basic types, i.e., fibrous microporous SiO_2, fibrous SiO_2/Al_2O_3, fibrous ZrO_2, fibrous carbon, foamed SiO_2, foamed carbon, and multilayer. Unfortunately there was practically no experimental data available from any source for the conditions of interest to us. Accordingly, a thorough testing program was initiated to obtain sufficient data to select the best materials, and then to generate the required design data for these materials.

Thermal conductivity tests were used as the primary screening tool, with vacuum guarded hot plate measurements (ASTM-C177-76) being performed on all the materials to

determine their relative thermal efficiencies. The more promising materials were also evaluated in xenon and helium atmospheres.

All the load bearing candidate materials had stress/strain curves run at room temperature, with the more promising ones then being subjected to long term (between 300 hour and 3500 hour) load relaxation tests at room temperature and in-gradient at generator conditions.

The finally selected load bearing materials (Min-K 1400 and CBCF-3) were then subjected to a cold vibration to generator levels in generator size and configuration. A set of long term in-gradient tests were run on these materials in a smaller size, to check the effect of such conditions on thermal and load bearing properties.

The selected multifoil side (non-load bearing) insulation was also evaluated experimentally. There were initially some fears expressed that the thin (0.0003") Mo foil might not withstand vibration, and that the ZrO_2 powder coating might be shaken off and reduce the insulation effectiveness. Therefore, a vibration test was performed to evaluate the insulations' mechanical stability.

All of the insulations have been evaluated for compatibility. Calculations of free energies were made, and where questions were raised, experimental checks were undertaken. TES, ORNL, BCL, 3M, JPL, and GA all cooperated in this area. Included in this effort was a study of outgassing characteristics of the materials and the development of outgassing procedures.

2.0 BULK INSULATION THERMAL CONDUCTIVITY EVALUATION

Direct measurements of thermal conductivity in vacuum, xenon, and helium environments were used as the primary screening tool on those insulations selected as a result of the literature survey. These tests were initially performed at Dynatech R/D Co., Cambridge, Mass. on a subcontract basis. More recent work has been performed at Teledyne Energy Systems using an apparatus built by Dynatech.

The test technique used was the guarded hot plate technique (ASTM C177-77). All samples were 20 cm diameter and approximately 2.5 cm thick. The results of each test represent the average thermal conductivity of two samples measured over the inner 10 cm of the sample. (Ref. 2).

The apparatus at Dynatech R/D Co., was equipped with a hydraulic ram which allowed the testing of all the load bearing candidates at an applied load of 40 psi. This is close to the minimum load required on the generator end plugs at launch. The results of these tests agreed very well with earlier tests at essentially no load conditions, indicating that the application of relatively high loads on the end plugs will cause no noticeable change in the insulation thermal conductivity.

2.1 Materials

The thermal insulation materials tested in this program are listed in Table 1. The Min-K and Microtherm materials consist of sub-micron size silica particles strengthened by silica fibers and containing opacifying agents (TiO_2 in Min-K and Cr_2O_3 in Microtherm) to minimize radiative heat transmission at high temperatures. The Min-K TE 1400 and 1800 have the same basic composition, but one of the fiber components is heat treated prior to mixing. Glasrock is an open cell fused silica foam, and the RVC materials are open cell vitreous carbon foam. The remainder of the materials consist of fine fibers (1 to 9 μm diamter by 0.02 to $\sim$1 cm long) with various binders to add strength and regidity, (except for the Fiberfrax which has no binder). The CBCF-1, -3, and -4 were made from a starting stock of rayon fibers, while the CBCF-5 and -6 used a polyacryllonitrile (PAN) fiber. These latter were manufactured and tested when it became apparent that sufficient quantities of uniform fiber rayon might not be available in the future.

TABLE 1

INSULATION MATERIALS SELECTED FOR STUDY

Material	Type	Nominal Density g/cc	Nominal Composition wt.%	Manufacturer (Ref. 3)
Min-K TE 1400	Micropore	.32	83.9 SiO_2 - 15.8 TiO_2	Johns-Manville
1800	Micropore	.32	83.9 SiO_2 - 15.8 TiO_2	Johns-Manville
2000	Micropore	.32	83.9 SiO_2 - 15.8 TiO_2	Johns-Manville
Microtherm 20 CR	Micropore	.32	62 SiO_2 - 3.2 Al_2O_3 - 32 Cr_2O_3 - 1.8 Fe_2O_3	Micropore Insulation Ltd. Worcestershire, England
Cotronics 360 HS	Fiberboard	.48	48 SiO_2 - 52 Al_2O_3	Cotronics Corp.
CBCF-1	Fiberboard	.27	99 + C (rayon base)	ORNL
-3	Fiberboard	.25	99 + C (rayon base)	ORNL
-4	Fiberboard	.13	99 + C (rayon base)	ORNL
-5	Fiberboard	.28	99 + C (poly-acryllo-nitrile base)	ORNL
-6	Fiberboard	.14	99 + C (poly-acryllo-nitrile base)	ORNL
ZYFB-3	Fiberboard	.50	92 ZrO_2 - 8 Y_2O_3/HfO_2	Zircar Products
Fiberfrax 660 H	"Paper" (felt)	.19	47.6 SiO_2 - 51.7 Al_2O_3	Carborundum
Glasrock 30	Foam	.48	99.6 SiO_2	Glasrock
RVC	Foam	.05	99 + C	Chemotronics
RVC-4	Foam	.11	99 + C	Chemotronics

2.2 Results

The experimental results are summarized in Table 2 and presented in Figures 1 to 4 for ease of comparison.

2.2.1 Vacuum

The micropore materials as a group yielded the lowest values of λ over the entire temperature range (Figure 1). The fibrous materials were somewhat higher and covered a much wider range of conductivities. These materials exhibited a very pronounced dependence upon density (CBCF-4 vs CBCF-3, CBCF-6 or CBCF-5 and Fiberfrax vs. Cotronics). For materials in the same density range they behave as would be expected from the base materials ($ZrO_2 < Al_2O_3/SiO_2 < C$). The foamed materials show reasonable values of λ near room temperature, but their insulation effectiveness decreases rapidly with increasing temperature. This is mostly due to direct transmission of radiant energy through the unopacified silica in the Glasrock, and to reflection through the open pore systems of the RVC's. The clean glassy surface of the carbon should lead to the transfer of large amounts of radiant energy by specular reflection through these open pores. The crossover of the conductivity of the less dense RVC-Std material at $\sim 500°C$ could be attributed to the very open pore structure of this material allowing more direct radiation losses with fewer reflections to quickly over-compensate the lower solid conduction term.

2.2.2 Outgassed Samples

Several samples of Min-K TE-1400 were outgassed according to SIG 30064 which requires the soaking of the oxide insulation at 870°C for 168 hours at 10^{-6} torr after an initial conditioning of 8 hours at 400°C and 10^{-3} torr. Samples of CBCF-3, CBCF-5, and CBCF-6 were outgassed according to TES Procedure SIG 30060 which requires a 32 hour soak at 1350°C and 10^{-5} torr.

TABLE 2

THERMAL CONDUCTIVITY (W m^{-1} K^{-1})

Material	Temp. (°C)	Vacuum (10^{-4} torr)					Xenon (0.9 atm)					Helium (1 atm)				
		200	450	650	900	1000	200	450	650	900	1000	200	400	650	900	1000
Min-K TE 1400		.0155	.0205	.0265	.0350°		.0170	.0230	.0290	.0415		.052	.074	.097	.123°	
Min-K TE 1400 (outgassed)		.0125	.017	.022	.026°											
Min-K TE 1800		.0140	.0200	.0270	.0350								.061			
Min-K TE 1800 (transverse)		.0179	.0240	.0325	.0465		.0205	.0305	.0420	.0620		.058	.0805	.105	.140	
Min-K 2000		.0172	.0250	.0375	.0615°							.058	.067	.0775	.099°	
Microtherm 20 CR		.0125	.0250	.0415	.0770							.033	.048	.0636	.099	
Fiberfrax 660 paper		.0066	.020	.032	.063		.0160	.0325	.048	.088°°						
Cotronics 360 HS		.038	.052	.071	.134		.063	.083	.105	.171		.285	.405	.520	.705	
Glasrock 30		.105	.155	.215	.345							.460	.640	.805	1.080	
RVC		.046	.120	.250	.570											
RVC-4		.080	.130	.200	.375		.095	.180	.295	.550		.345	.545	.725	1.010	
CBCF-1		.135	.160	.165	.165°	.170#	.175	.210	.270	.355°	.465	.420	.550	.665	.800°	0.940
CBCF-3		.100	.115	.130	.155°	.180	.130	.165	.195	.230°	.265	.310	.400	.490	.600°	.710
CBCF-3 (outgassed)		.0715	.0935	.115	.135	.158										
CBCF-4		.019	.0305	.044	.063°	.083	.040	.0645	.0955	.135°	.185	.220	.385	.600	.940°	1.25
CBCF-5 (outgassed)		.125	.215	.300	.395	.485										
CBCF-6 (outgassed)		.0355	.0575	.071	.099	.115										
ZYFB-3		.0295	.0425	.057	.076°	.0945	.0545	.082	.115	.160°	.205	.305	.405	.510	.640°	.760
ZYFB-3 (transverse)							.070	.110	.155	.215°	.280					

° 850°C °° 850°C # some evidence of reaction

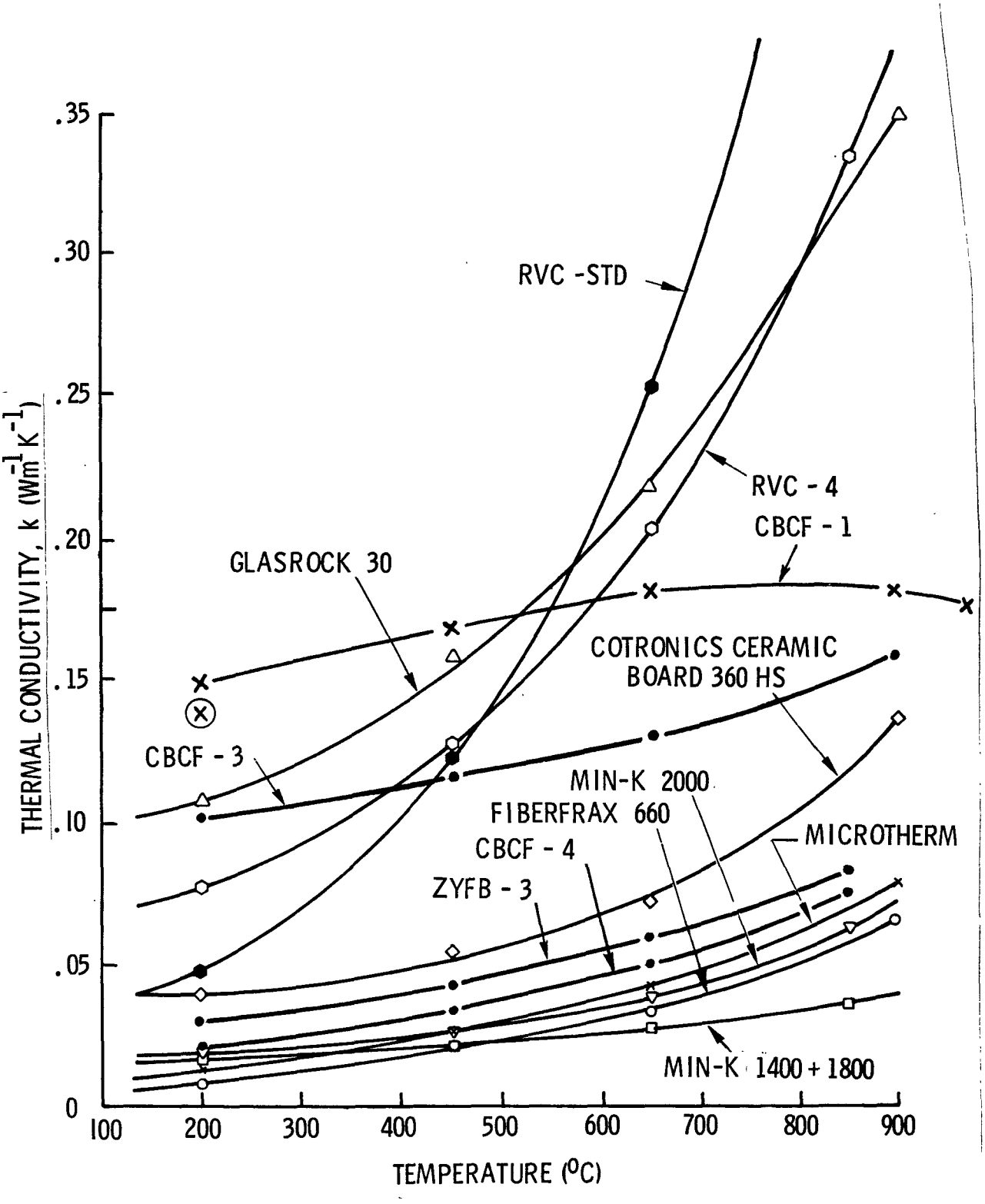

Figure 1. Thermal Conductivity in Vacuum

The thermal conductivities of all these samples were then determined in vacuum in the same equipment used for the virgin samples. The same Min-K TE 1400 and CBCF-3 samples were used in both tests. The results of these tests are compared in Figure 2.

Relatively little effect was observed in the Min-K TE 1400. The data shows a slight decrease in thermal conductivity. The test samples did have some signs of incipient delamination which could lead to a lowering of the thermal conductance. However, since the difference between the outgassed and un-outgassed measurements is generally within the range of experimental error, it is difficult to decide whether or not this effect is real.

The CBCF-3 samples showed a somewhat greater decrease in thermal conductivity. These samples also had a slight decrease in density as a result of outgassing, indicating a possible loss of binder material. If such is the case, the solid conduction term would be smaller, resulting in a decrease in λ.

Both of the PAN fiber materials were measured in the outgassed condition only. Their conductivities were expected to be similar to those of CBCF-3 and -4.

The CBCF-6 material yielded a curve roughly paralleling CBCF-4 but substantially higher. It is possible that a decrease in density could yield a lower conductivity. However, the actual position in the minimum of the λ vs ρ curve is not known.

The CBCF-5 data, on the other hand, was not only much higher than that of CBCF-3, but it exhibited a temperature dependance more like that of the glassy foam RVC materials than like other fibrous materials. At the present time we have no explanation for such atypical behavior, especially since the supposedly similar CBCF-6 PAN fiber material follows the "normal" fibrous insulation pattern exhibited by the rayon based CBCF-4 so well. It was suggested that the high temperature (1600°C) required to drive off the nitrogen could have led to graphitization of the fibers. However, x-ray scans failed to uncover any significant graphitic character in the material.

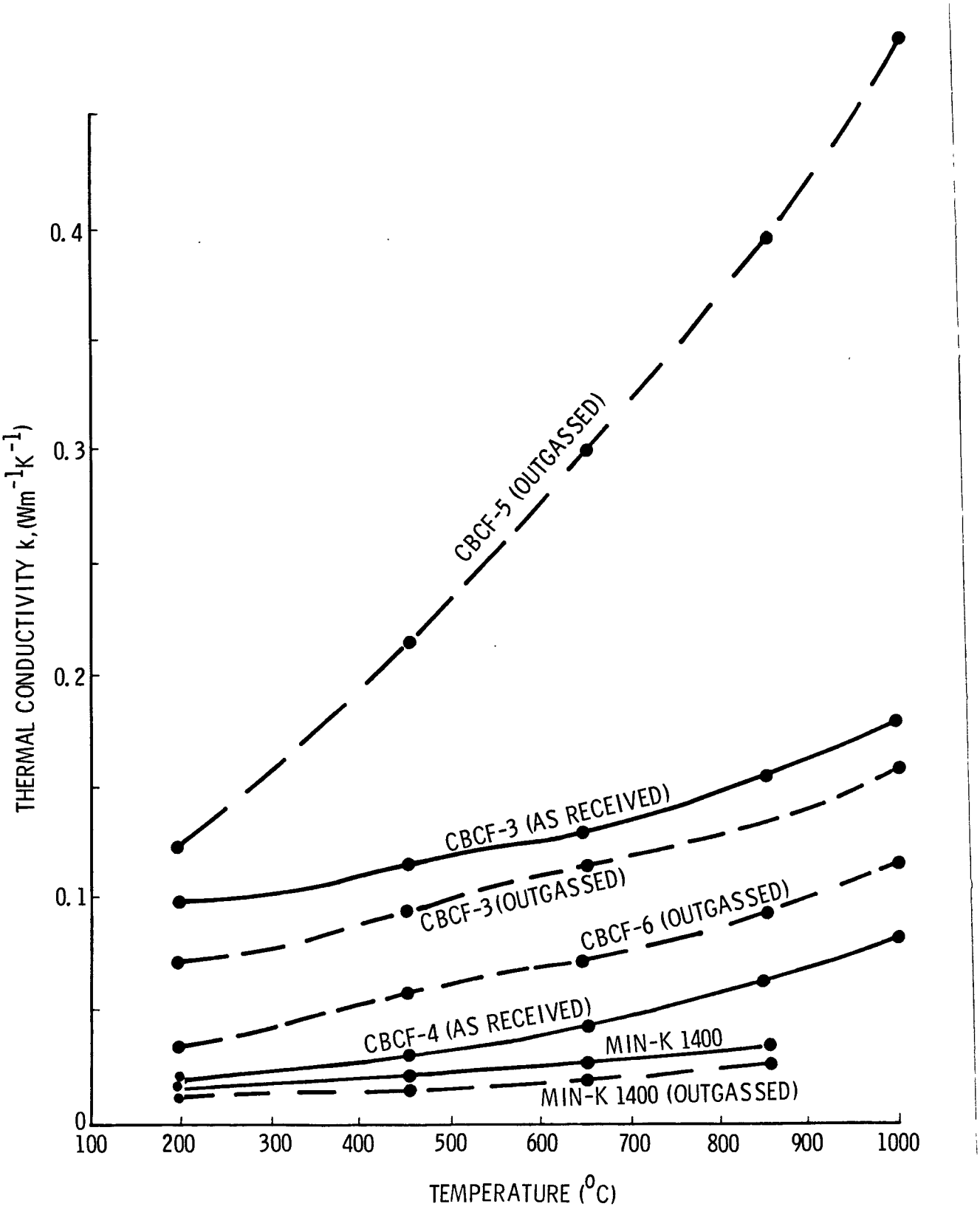

Figure 2. Thermal Conductivity of Outgassed Materials

2.2.3 Xenon

This gas produced relatively little effect on the conductivity of the micropore materials, as exemplified by the Min-K 1800 (Figure 3). The fibrous and foamed materials generally showed a 50 to 100% increase is due to gaseous conduction. This was expected since these materials present a much more open path to the xenon atoms than do the micropore materials.

The two broken line curves illustrate the increase in λ observed in the direction parallel to the main fiber orientation (perpendicular to the pressing direction during fabrication of the materials). These show increases of 20 to 50% rather than the 5 to 10% estimated by the manufacturers. This confirms the effect observed earlier at low temperatures on Min-K 20000 (Ref. 4). The CBCF materials have previously been shown to have a λ roughly 250% higher in this direction(Ref. 5). Therefore one must be careful in the use of one dimensional calculations for design approximations.

2.2.4 Helium

In this case the obvious superiority of the micropore materials is especially pronounced (Figure 4). The overall effect of an atmosphere of helium is an increase of less than 0.1 $Wm^{-1}K^{-1}$ over the entire temperature range for these materials, while the fibrous boards and foam material jump 0.5 to over 1.0 $Wm^{-1}K^{-1}$ higher with the increase being most pronounced at the highest temperatures. The CBCF-4 increased substantially more than the CBCF-1 or CBCF-3. This is attributable to its significantly more open structure which allows a much greater contribution through convection losses in the helium. The very high values for Glasrock and RVC-4 also point to the dominance of helium conduction through the open pores. The reversal of positions of Microtherm and Min-K with respect to their relative performance in vacuum may or may not be real. Past experience has shown that these materials with their extreme surface to volume ratios present serious

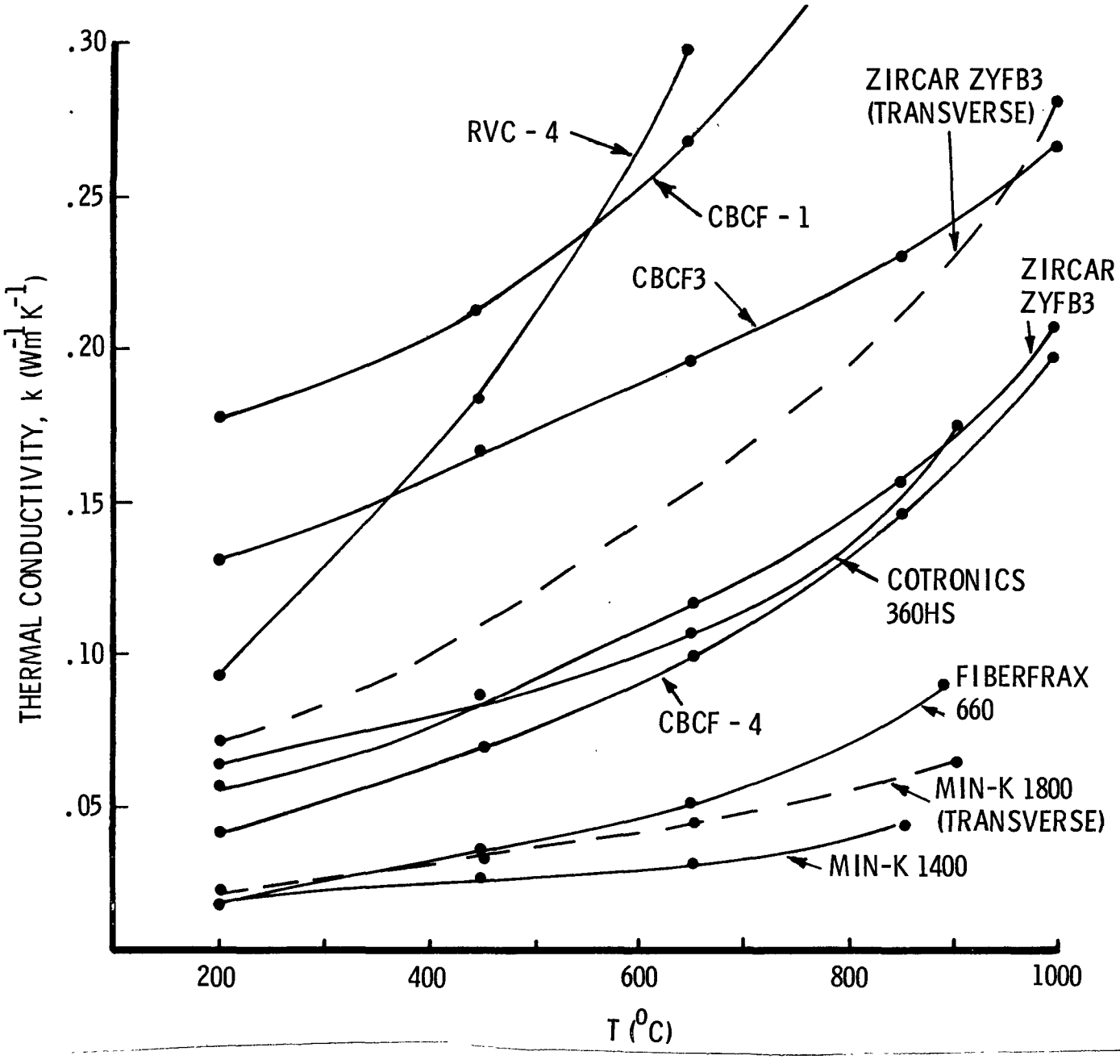

Figure 3. Thermal Conductivity in Xenon

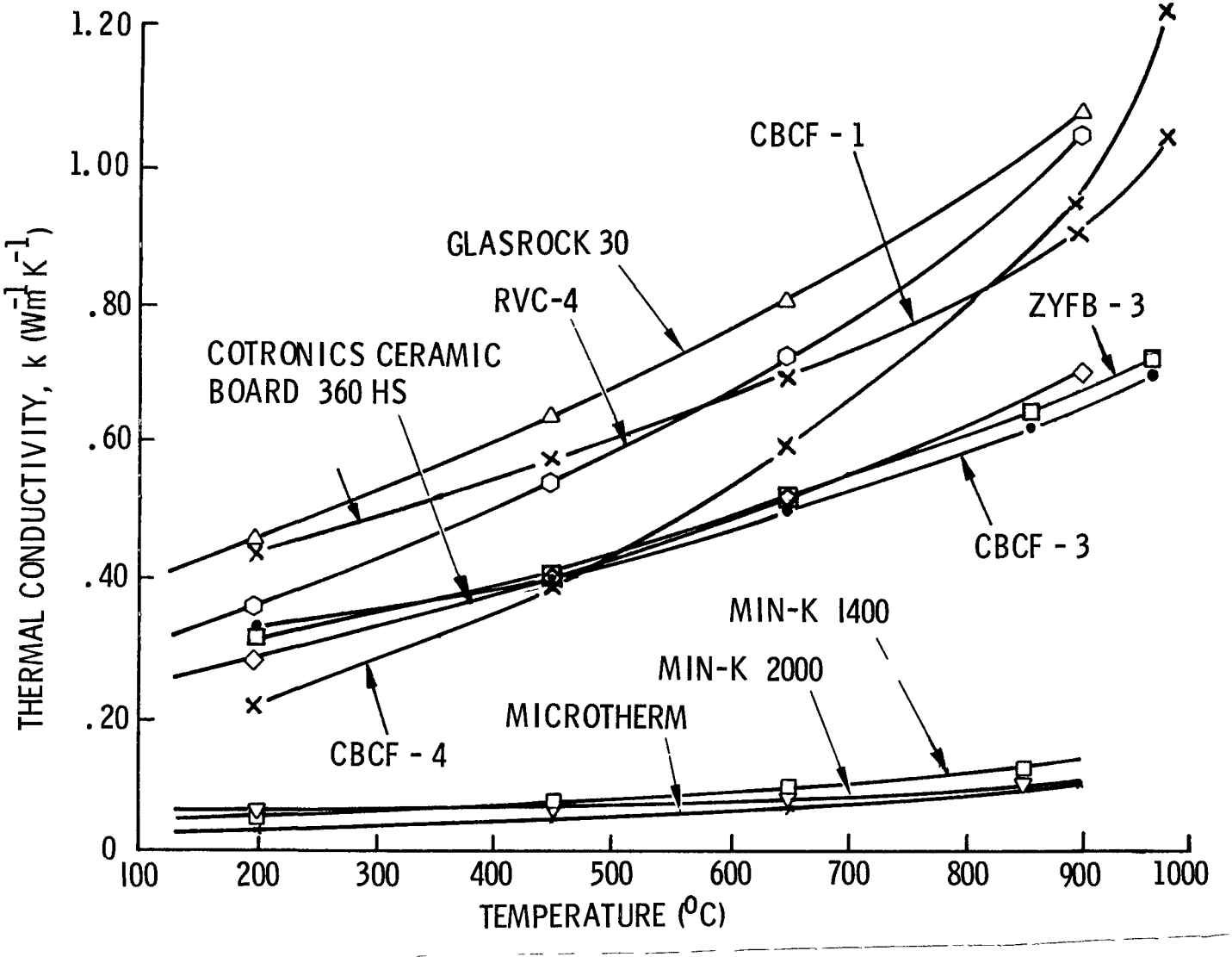

Figure 4. Thermal Conductivity in Helium

problems in complete evacuation and thorough gas exchanges. This effect was considered and great care was exercised to allow sufficient time at each temperature for equilibrium to be reached (as much as four days in one instance) however there is still a possibility that some of the data may be slightly off since there was no way of inserting a pressure transducer within the pores of the sample.

2.2.5 Air

Since most thermal conductivity data reported in the open literature is obtained in an air environment, it was considered appropriate to check these materials in air so as to supply a method of cross-comparing them with other insulations. Accordingly, a series of measurements were made up to 200°C using a heat flow-meter which has been shown to have a comparable accuracy to the guarded hot plate in this temperature regime. These results are given in Table 3 and Figure 5. They follow the trends observed in the other test environments very well, although the poor performance of the foam materials at higher temperatures isn't very obvious since the gaseous conduction and radiation components haven't become dominant yet.

2.3 Discussion

The data presented above were used to make the initial selection of insulations for use in the ground demonstration system of the selenide isotope generator. The original choices were Min-K TE 1400 for the end support sections operating below 800°C and Cotronics 360 HS for the higher temperature areas. However the Cotronics failed in later vibration tests and the somewhat higher λ material CBCF-3 was chosen to replace it. Microtherm 20CR was essentially equivalent to Min-K TE 1800, but the chromium oxide opacifier in it was judged to be potentially more of a compatibility problem than the titania in the Min-K.

For the side (non-load bearing) insulations Zirconia ZYFB-3 and Min-K TE 1800 were selected on the basis of low λ. The extreme fragility of the zirconia board led to

TABLE 3

THE APPARENT THERMAL CONDUCTIVITY OF NINE HIGH TEMPERATURE INSULATION MATERIALS IN AIR

Material	Apparent Thermal Conductivity, $Wm^{-1}K^{-1}$		
	20	100	200C
Fiberfrax 660	0.034	0.039	0.050
RVC Standard	0.044	0.060	0.082
RVC-4	0.071	0.086	0.100
Min-K 1400	0.025	0.027	0.029
Min-K 2000	0.026	0.028	0.031
Microtherm	0.022	0.023	0.026
Cotronics	0.078	0.087	0.098
Glasrock 30	0.125	0.142	0.168
Zircar	0.075	0.084	0.099

TEST PROCEDURE: ASTM C518-76. "Steady-State Thermal Transmission Properties by Means of the Heat Flow Meter."

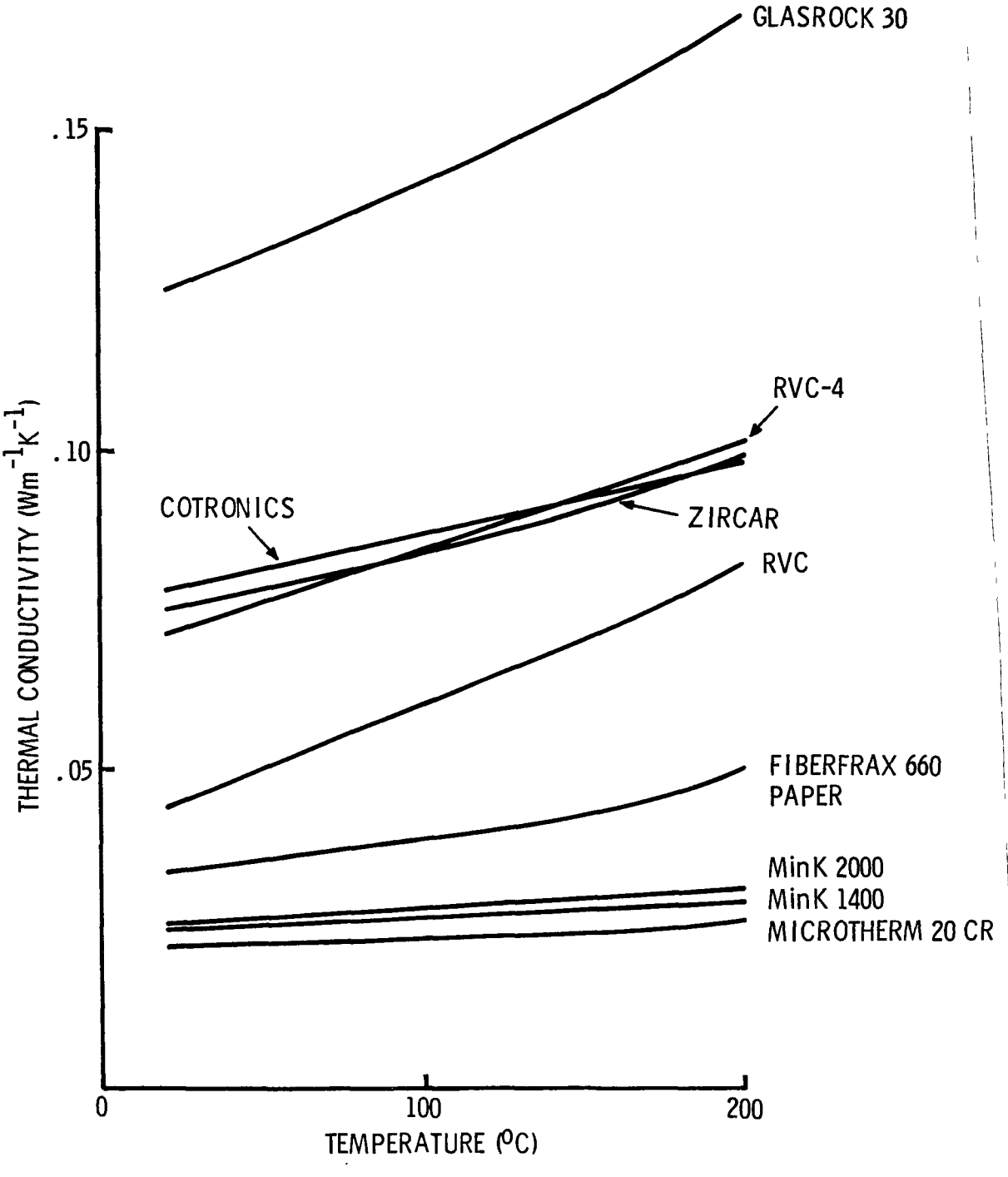

Figure 5. Thermal Conductivity in Air

the development of CBCF-4 as a low density back-up material. Its structural superiority and lower λ in vacuum and xenon eventually led to it being chosen as the preferred material for the side areas above 850°C.

The data generated in the program are expected to be very useful in the comparison of these materials with the many others available and to aid investigators in estimating values of λ for other materials in exotic environments by making use of cross reference charts such as presented in Table 4. By judicious comparison of structurally similar materials reasonable estimates of λ values can be made at any given temperature in any of these environments based on actual data available in air or any of the other environments.

TABLE 4

COMPARISON OF THERMAL CONDUCTIVITIES OF VARIOUS INSULATION MATERIALS IN DIFFERENT ENVIRONMENTS @ 200°C

Material	Apparent Thermal Conductivity ($Wm^{-1}K^{-1}$)			
	Vacuum	Xenon	Air	Helium
Min-K 1400	.0155	.0170	.029	.052
Min-K 1800	.0140			
Min-K 2000	.0172		.031	.058
Microtherm 20 CR	.0125		.026	.033
Fiberfrax 660 Paper	.0066	.0160	.050	
Cotronics 360 HS	.038	.063	.098	.285
Glasrock 30	.105		.168	.460
RVC	.046		.082	
RVC-4	.080	.095	.100	.345
CBCF-3	.100	.130		.310
CBCF-4	.019	.040		.220
ZYFB-3	.0295	.0545	.099	.305

Air Measurements: ASTM C518-76 (Heat Flow Meter)

All Others: ASTM C177-77 (Guarded Hot Plate)

3.0 LOAD BEARING TESTS

The insulation load bearing experiments in the SIG development program were designed to provide some critical, but generally unavailable, physical property data on the various candidate insulations. These data were factored in with thermal conductivity results to establish the prime candidates for generator design.

The elastic modulus of the insulation material was determined at room temperature and then in-gradient load relaxation tests were performed in inert gas environments. The load relaxation data were initially calculated from the results of a series of creep tests similar to those previously conducted at Martin-Marietta and at Johns-Manville (Ref. 6). However, when sufficient data had been collected to analyze critically, it became apparent that this technique was rather sensitive to small variations in several of the experimental steps.

Therefore, a modified fixture which used a strain gauge to measure the load relaxation more directly was substituted (Ref. 7).

3.1 Experimental Methods

3.1.1 Elastic Modulus Determinations

All elastic modulus determinations were made at room temperature (75 ± 5°F). All materials were tested using the creep test fixture (Figure 6). The stress was applied by means of a hydraulic ram and load cell which had been calibrated against a Dillon gauge. The strain was measured using a set of four height indicator gauges (2 reference and 2 on the sample). The test specimens were 2-1/2 x 2-1/2 x 2 inches, except for CBCF-3 where only 1" x 1" x 1" samples were available early in the program. Later 2" x 2" x 2" samples of the material became available and were tested.

3.1.2 Creep Tests

The creep tests were run in the same fixture as the elastic modulus tests. The

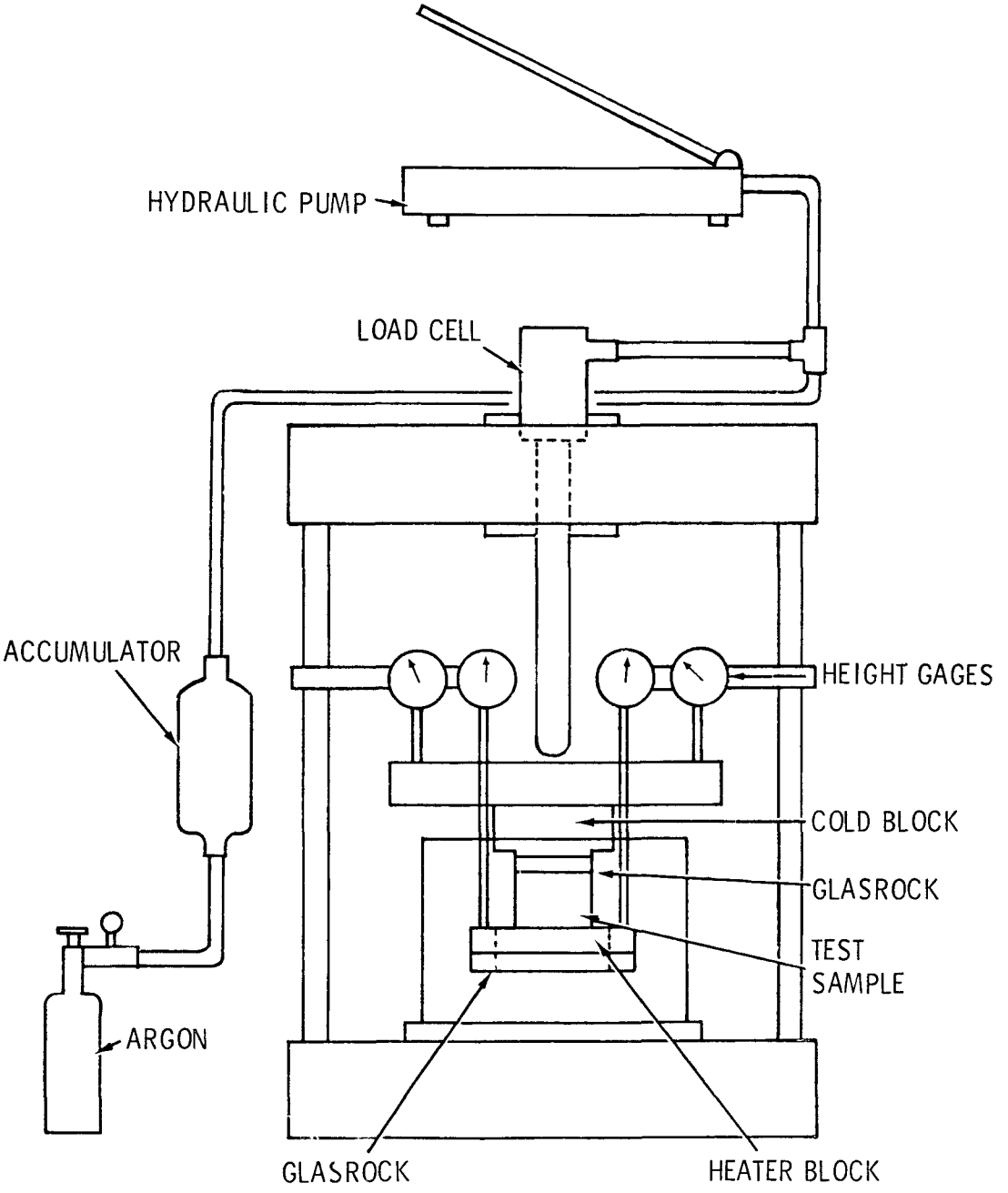

Figure 6. Creep Test Fixture Schematic

desired temperature gradient was established by means of a Mo heater in a graphite block at the hot face and a water-cooled chill block at the cold face.

The load relaxation characteristics of each material were obtained from a series of tests. The hot and cold face temperatures were fixed and a constant load was applied through the hydraulic ram/pneumatic accumulator system. Then the variation in compression as a function of time was noted. A series of such tests were run at 20, 50, 100, 150, and 200 psi. Data were generally collected for 1000 hours and then extrapolated on a log-log scale to 70,000 hours.

These results were then cross-plotted as % deflection vs load on a log-log scale pa parametric in time. Then the intersection of the initial deflection value with each of the lines was replotted to give the load relaxation curve for the material at the selected initial load.

3.1.3 Strain Gauge Tests

In this fixture (Figure 7) the heater block is firmly supported by solid zirconia rods to prevent relaxation of the supporting insulation. The initial load is applied through a stud-type strain gauge which is locked in position by a lock nut on the supporting threaded rod. The amount of load relaxation is then measured directly through the strain gauge.

3.2 Test Results

3.2.1 Modulus of Elasticity

The results of the room temperature modulus of elasticity determinations are given in Table 5. Nearly all of these materials exhibited an essentially linear response over the range tested. The major exception was CBCF-3 which yielded a series of curves, mostly "S" shaped. These are shown in Figure 8A for several one inch cubed samples and in Figure 8B for a series of 2 x 2 x 2 inch samples. The smaller samples yielded a much lower average value for the modulus than did the larger samples, probably due to edge effects being rather large compared to the total sample. The lower curve in Figure 8A was obtained after the sample had been subjected to loads of over 200 psi and had yielded.

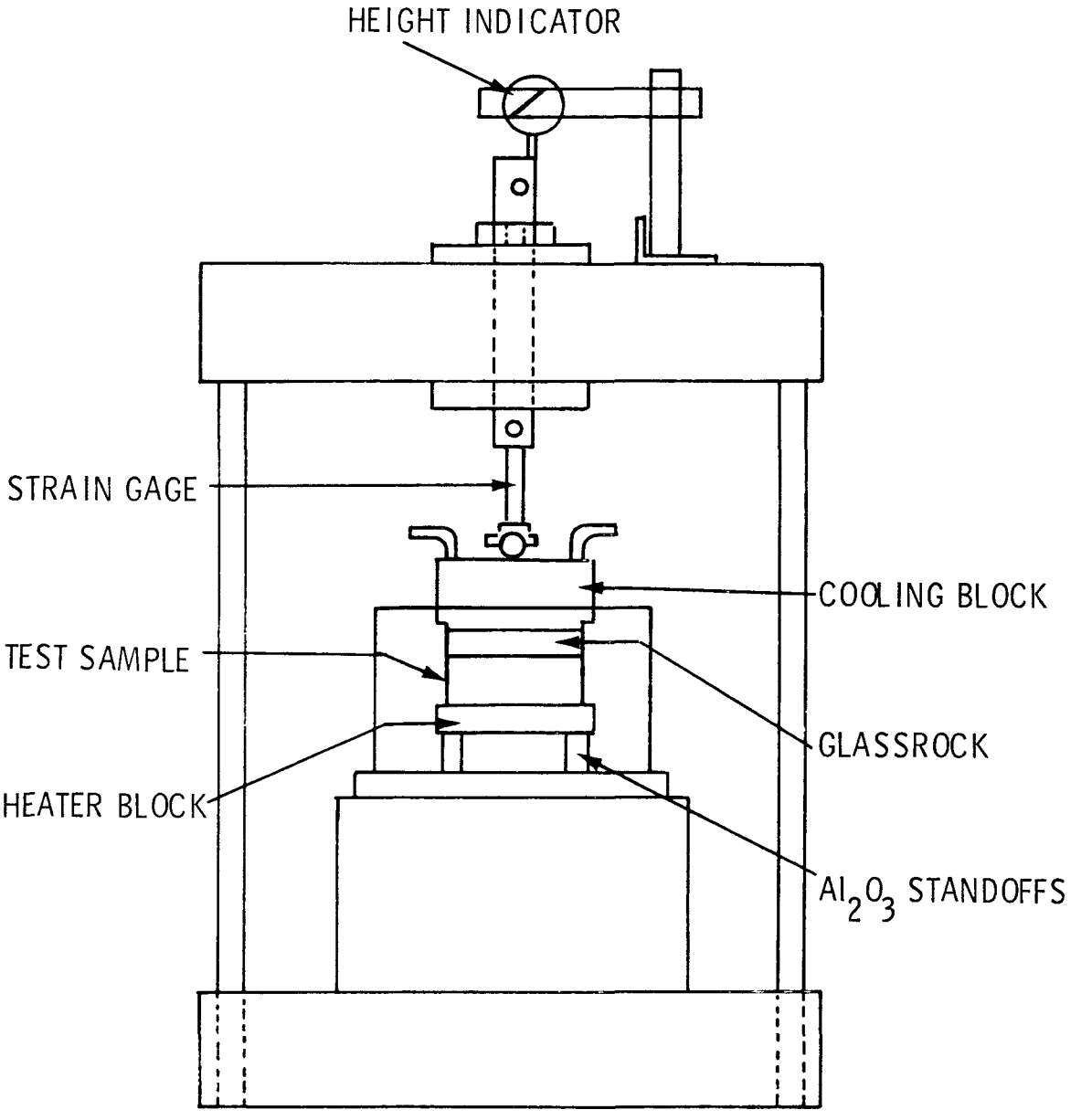

Figure 7. Load Relaxation Test Fixture

TABLE 5. MODULUES OF ELASTICITY AND LOAD BEARING CAPABILITY OF VARIOUS INSULATION MATERIALS AT ROOM TEMPERATURE

Material	Nominal Modulus of Elasticity (psi)	Maximum Load Level (psi)	Nominal Density (pcf)
Min-K TE 1400	2000	150	20
Min-K TE 1800	1950	150	20
Min-K 2000	3300	170	20
Microtherm 20 CR	1140	180	20
Cotronics 360 HS	4700	350	30
Glasrock 30	25000	300 (crush)	30
Zircar - ZYFB3		45	30
CBCF-3	Nonlinear	150	14
RVC-4		200 (crush)	7

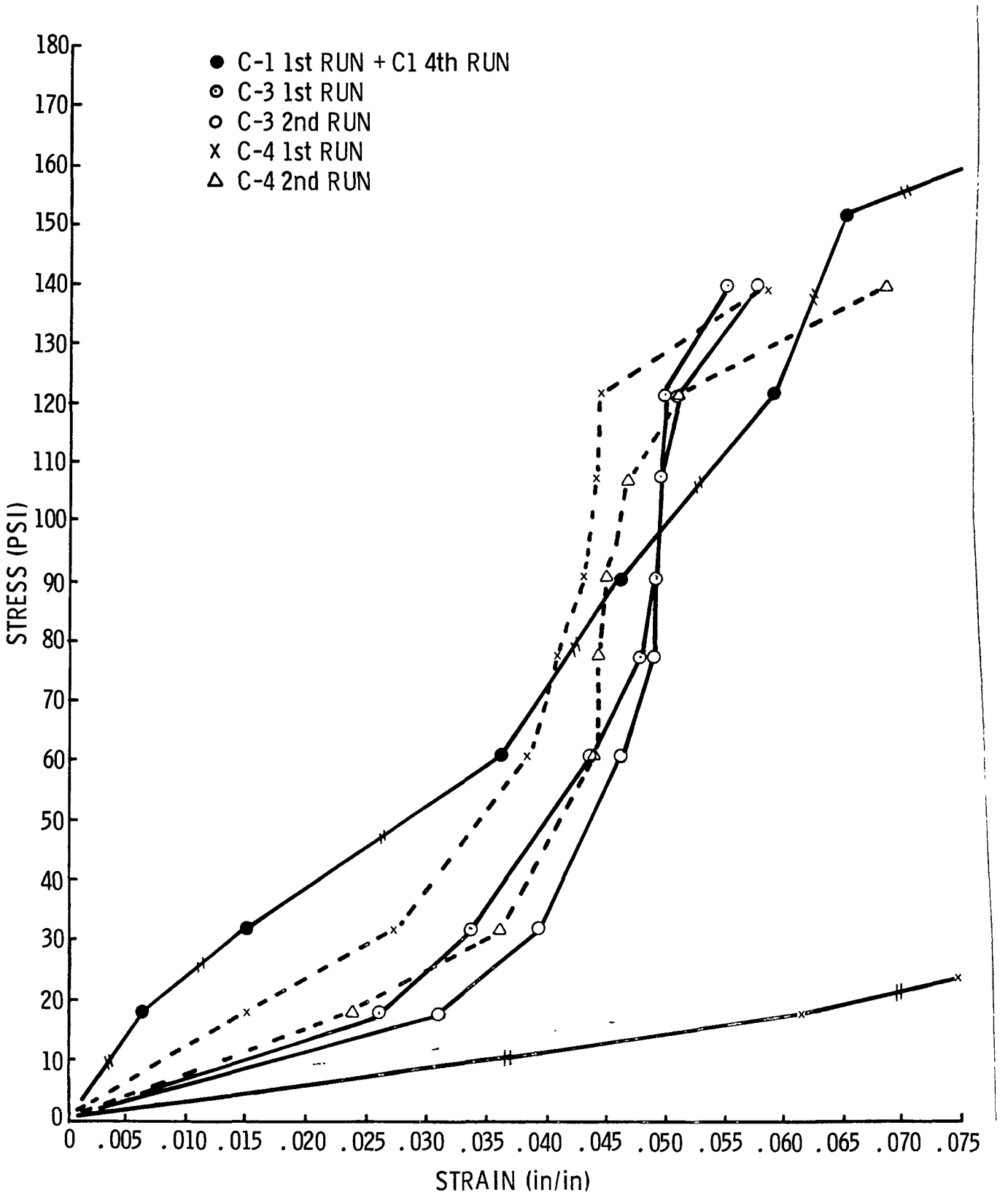

Figure 8A Room Stress vs. Strain for CBCF-3 (1"x1" Sample)

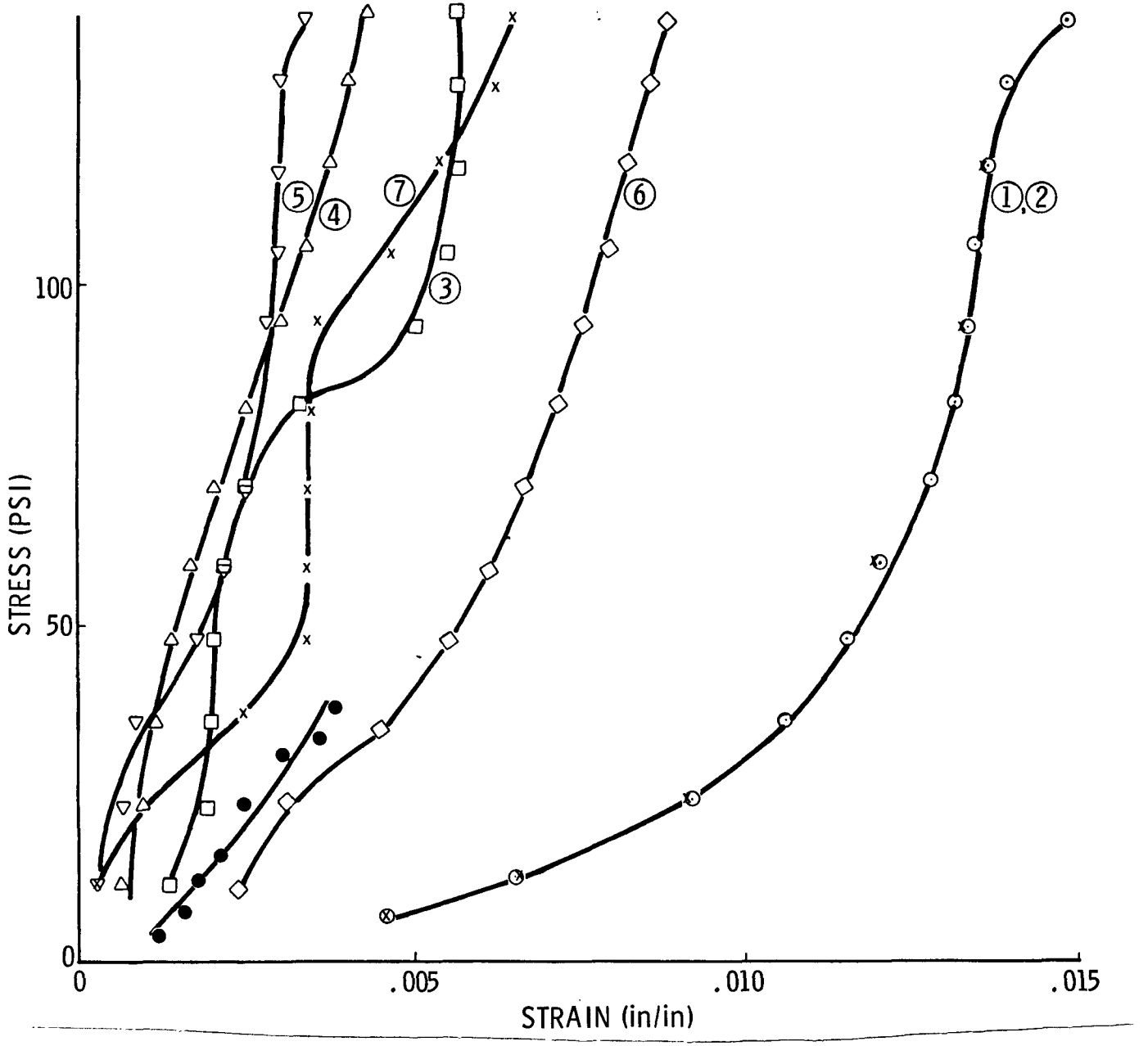

Figure 8B. Room Temperature Stress vs. Strain for CBCF-3 (2x2 Sample)

All tests after this were run only up to a maximum loading of 150 psi on this material.

The curves in Figure 8B represent the results from the larger samples in which edge effects (e.g., damage from cutting) would be relatively less important. Again these curves are generally non-linear. The average modulus of elasticity is much higher than the apparent value observed for the 1 inch cube samples. However the variation between samples is very large. Each of the curves shown was reproducible at least two times. The seven samples tested were from three different batches of CBCF-3. Curves 1 and 2 which overlap almost perfectly are for samples taken from one of the earliest billets of CBCF-3. They had a density of 0.25 g/cm^3. Samples 3,4, and 5 were from a later billet and they had densities of 0.29 g/cm^3. While samples 6 and 7 were from a third billet with a density of 0.27 g/cm^3.

Such wide scatter in the data from sample to sample make it very difficult to select good design data for load bearing applications.

3.2.2 Creep Tests

The initial program plan called for creep tests exclusively. However, when sufficient data were collected for analysis, it became apparent that the use of multiple samples in several tests, and the substantial data manipulation required to convert the results to effective load relaxation results, made the final results somewhat open to question. This meant that a large number of samples would be required to obtain statistically reliable results. Since each relaxation curve required four or five 1000-hour runs at each temperature, it was decided to switch to a new type test utilizing a strain gauge.

Several series of creep tests were completed for Min-K 1400, and the results are shown in Figure 9.

The load relaxation results for the second and third runs at 880°C hot face and the second run at 830°C and the only run at 800°C are shown along with data reported by Johns-Manville for 760°C. The cold face was held at ~150°C for all the tests.

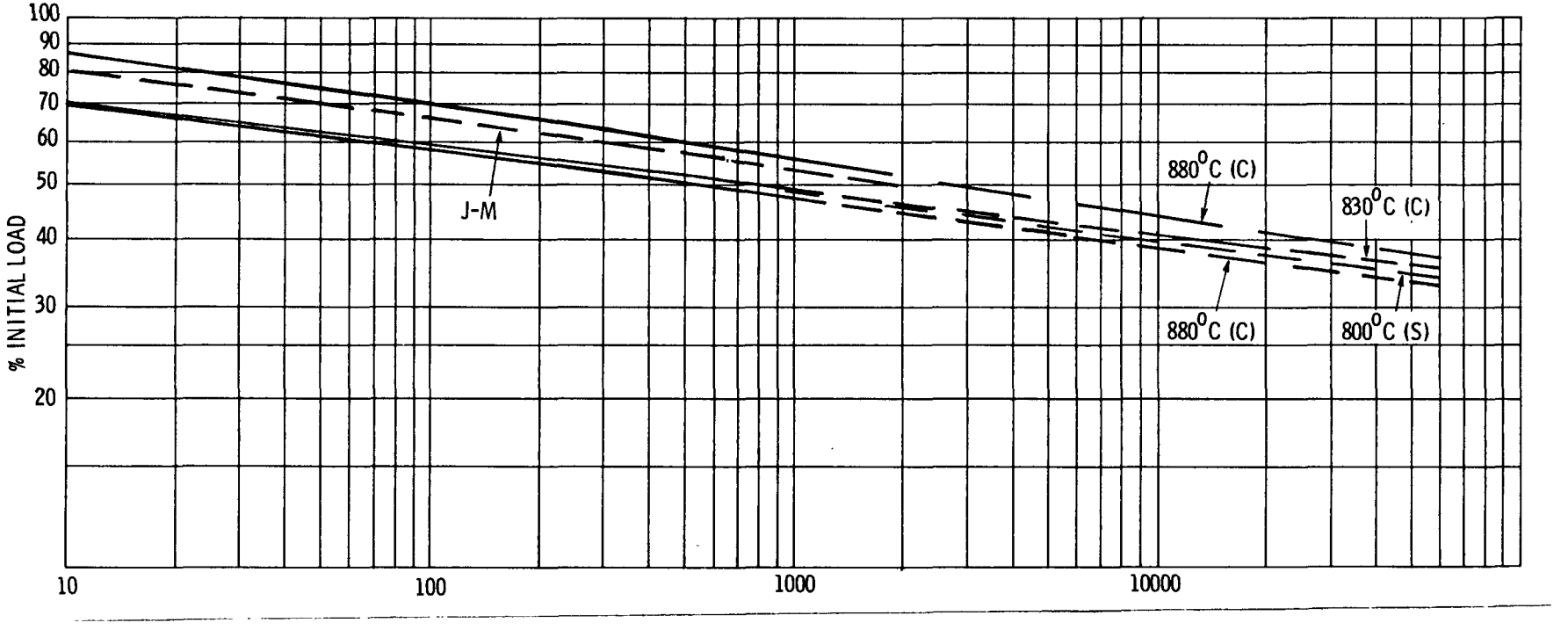

Figure 9. Load Relaxation of Min-K TE 1400

The first runs at 880°C and 830°C were discarded because of some variations in load which occurred during the tests and also because of some question as to the determination of the actual zero time load. (These data indicated between 45% and 67% of initial load remaining at 10,000 hours, while all of the other creep data and the strain gauge data clustered in the 40% to 45% area.)

Partial tests on Cotronics 360HS and Microtherm 20CR were left incomplete when these materials were dropped from consideration for use in the GDS.

3.2.3 Strain Gauge Tests

Four new fixtures which give more direct load relaxation type data were installed and several materials tested. These included Min-K 1400 at 800/150°C, Min-K 1800 at 900/150°C, and Min-K 2000 at 800/150°C. The results of these tests are given in Figure 10.

The Min-K TE 1400 showed a logarithmic load relaxation that agreed very well with the lower set of data generated in the creep test fixture. Min-K TE 1800 and Min-K 2000 were also tested in these fixtures with hot face temperatures of 900° and 800°C, respectively. Neither of these materials exhibited any good load bearing qualities at these temperatures as can be seen in Figure 10. At room temperature, neither of these latter materials showed any relaxation after 300 hours under a load of 100 psi. Min-K TE 1400 had still not relaxed after 1200 hours under load at room temperature.

Several later tests on Min-K TE 1400 which had been outgassed at 860°C for a week, yielded inconsistent results. Three samples relaxed at a rate somewhat faster than the unoutgassed Min-K TE 1400, but still slower than Min-K TE 1800.

Several tests were run to see if the samples could be pre-stressed, i.e., run in gradient until much of the initial relaxation had occurred, and then readjust the load to the original value. It was hoped that this would then allow the material to relax at the slower rate normally encountered after some relaxation has occurred. The results of one of these

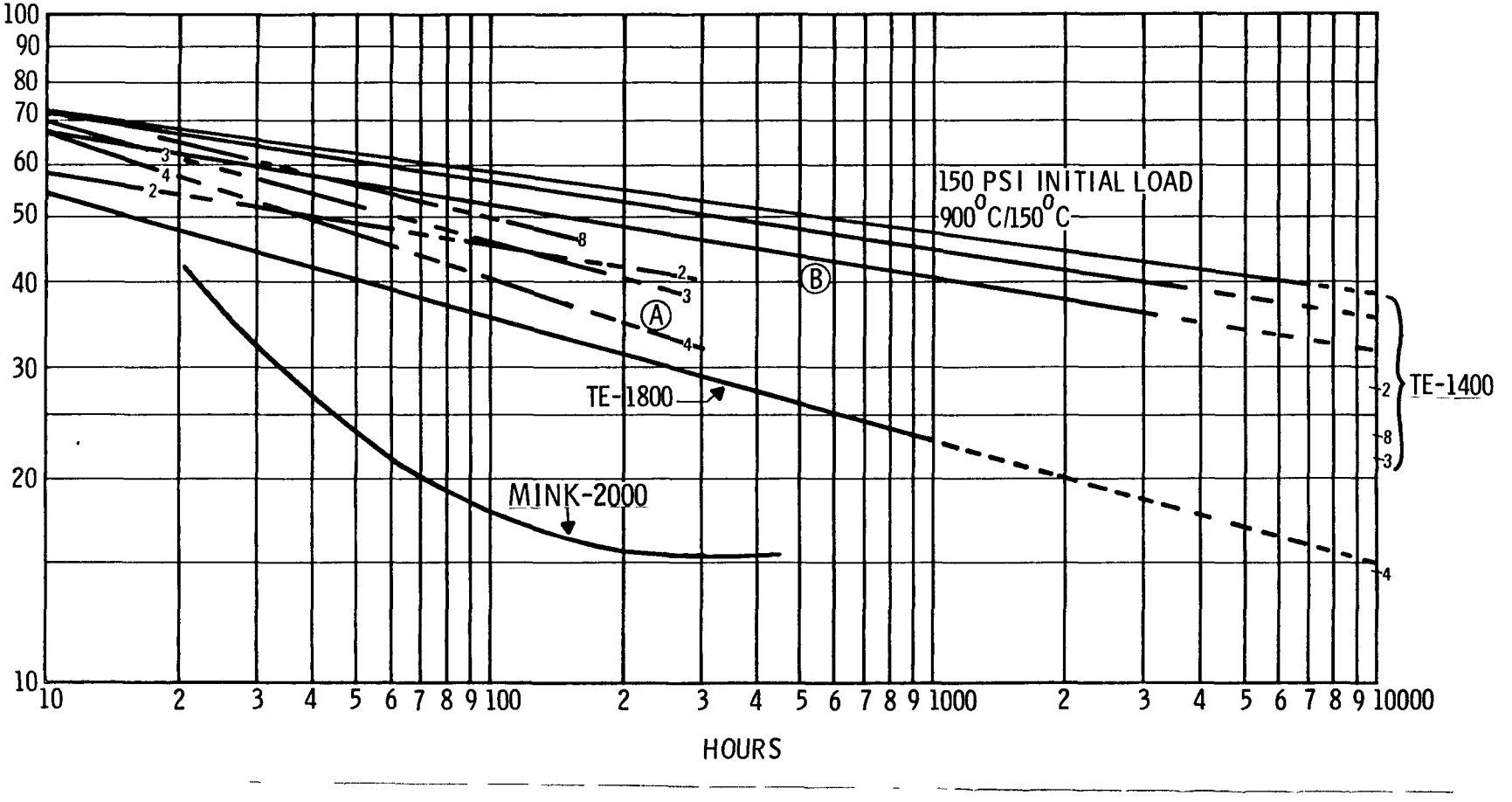

Figure 10. Min-K Load Relaxation From Strain Gauge Data

tests is shown in Figure 10. The line marked (A) represents the relaxation of an outgassed Min-K TE 1400 sample as initially loaded. After 270 hours the load was readjusted to the original level and the relaxation then proceeded as in (B). The actual physical change in the test fixture involved moving the strain gauge down onto the sample by only 0.0015" to re-establish the initial load.

It thus appears as if a large amount of the increased load relaxation in the outgassed samples may be the result of a small surface change, and can be recovered by a preloading treatment at temperature. More tests are needed to confirm this however.

It is uncertain whether the scatter in the outgassed experiments is a result of Min-K material differences or arise from slightly different reactions to the outgassing environments.

The CBCF-3 samples showed similar scatter among the outgassed samples as can be seen in Figure 11. The data for lines A and B were for the initial CBCF-3 material and were obtained on 1 x 1 x 1 inch samples. The C and D curves represent data obtained on 2 x 2 x 2 inch samples from later batches of Min-K. These were outgassed samples. Sample D was found to have delaminated sometime during the test. It is not known whether this caused the rapid drop in the first 10 hours of testing or not. However this does seem likely, since from this time on the slopes of the "strong" and the "weak" samples are nearly indentical. It is quite probable that resetting this sample to its initial load point would have produced a relaxation very similar to that of sample C.

3.3 Discussion of Results

The prime end disc candidates to emerge from these tests were Min-K 1400 for temperatures below 810°C and CBCF-3 for higher temperatures.

Both the creep tests results and the strain gauge tests agreed fairly well with earlier Johns-Manville date. The scatter on the creep test data was rather large, but this could be expected since each curve was derived from composite data on four individual samples, and depended on curve fitting techniques and a very precise "zero time" measure-

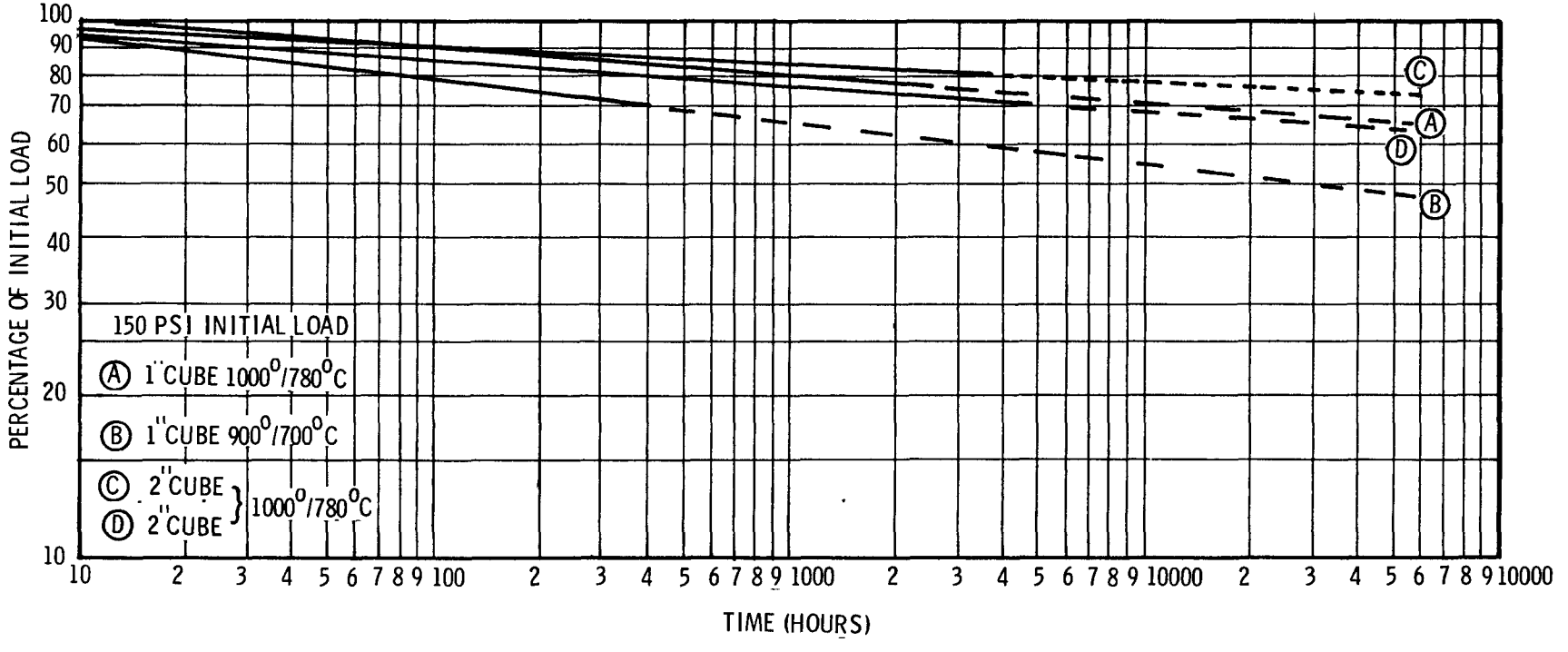

Figure 11. Load Relaxation of CBCF-3

ment on each of these samples. This latter was made all the more difficult since the material experienced its greatest relaxation upon the initial application of load at temperature.

The strain gauge test results were much more directly converted to load relaxation values, and had the advantage of using a single sample for a complete determination. The main source of error in this test was the differential thermal expansion between the various components of the fixture and the sample.

Both the Min-K 1400 and the CBCF-3 were shown to retain enough of their initial load bearing capability to enable the system to withstand launch vibration loads for at least one year after fueling in the as manufacture condition. Their relaxation rate may increase somewhat after being outgassed according to SIG procedures, especially in the case of Min-K TE 1400. However, preliminary tests indicate that much of this change can be recovered by "re-stressing" the outgassed samples for a few days before loading them in the generator.

4.0 MULTILAYER INSULATIONS

When the SIG program was switched to an all vacuum generator, multilayer insulation systems became much more attractive for use in the non-load bearing sections. This type insulation has several advantages over fibrous materials under these conditions, including lower thermal conduction, less outgassing, and more efficient generator pumpdown.

4.1 Materials

The basic considerations followed in the selection of materials were effective thermal conductance, density of foil materials, vapor pressure of foil materials at operating temperatures, density of separator material, vapor pressure of separator material, free energies of foil and separator materials for reaction with other components of the generator, emissivities of the materials as fabricated, previous experience with systems at high temperatures and long term stability.

Both cloth spacers (Linde/MHW approach) and particle separators (TECO approach) were evaluated. Some of their relative advantages and disadvantages for this program are compared in Table 6. The particle separator system was finally chosen mainly because of the weight factor and the ability of matching its overall thickness to the height of the thermoelements. (Refs. 8,9).

A number of metals were considered for the multifoil design. Some of their more pertinent properties are listed in Table 7. Temperature limitations because of either melting or vaporization problems led to the elimination of Al, Ti, Ni, Cu, Pd, Au from hot side use. Although Zr and Nb have good physical properties, they are such excellent getters that it was feared their emissivities might be drastically altered by reaction with outgassing products. Rh, Ta, W, Re, Pt and Ir have too high densities, and, in some cases, were too hard to obtain in long thin foils needed for practical assembly.

TABLE 6

Comparison of Two Types of Multilayer Insulation

PARTICLE SPACERS (TECO)

Advantages

- Free Pumping
- Minimal Outgassing
- Adjustable Spacing
- Lowest Weight
- BIPS/KIPS/Furnace Experience
- Recent Experience

Disadvantages

- Minimal Vibration Data to Date

CLOTH SPACERS (LINDE)

Advantages

- Easily Controlled Layup
- MHW Experience

Disadvantages

- High Weight
- More Outgassing
- Stock Thickness Greater Than T/E Height
- 50% Increase in K with ZrO_2 Cloth
- Wire Mesh for Getter Clearance

TABLE 7

Selected Metals Properties

Metal	Density (g/cc)	T_H °C	Vap'n Loss (μm/Hr) at (T °C) (Ref. 10) 500	800	1100
Aluminum	2.70	660	1.9×10^{-3}	*	*
Titanium	4.51	1668	2.9×10^{-12}	6.2×10^{-4}	29.3
Zirconium	6.49	1852	1.5×10^{-21}	1.1×10^{-10}	1.4×10^{-4}
Niobium	8.4	2415	9.7×10^{-33}	3.4×10^{-18}	5.0×10^{-10}
Nickel	8.9	1453	2.5×10^{-9}	0.080	1303
Copper	8.96	1083	5.8×10^{-5}	68.6	*
Molybdenum	10.2	2610	3.4×10^{-23}	4.2×10^{-12}	7.1×10^{-6}
Palladium	12.0	1552	1.1×10^{-8}	0.12	1137
Rhodium	12.4	1966	6.5×10^{-18}	5.8×10^{-8}	.023
Tantalum	16.6	2996	5.6×10^{-34}	1.7×10^{-19}	2.2×10^{-11}
Gold	19.3	1063	6.7×10^{-6}	13.0	*
Tungsten	19.32	3410	2.8×10^{-35}	1.2×10^{-20}	2.1×10^{-12}
Rhenium	21.0	3180	10^{-34}	10^{-19}	10^{-11}
Platinum	21.4	1769	7.5×10^{-18}	4.7×10^{-8}	0.015
Iridium	22.5	2454	1.4×10^{-22}	3.2×10^{-11}	6.5×10^{-5}

*Molten at this temperature

Nominal foil thickness would be 7-25 μm.

Molybdenum was selected as the best overall compromise material. It exhibits minimal weight loss at the highest operating temperatures, is not too reactive. Although density is somewhat on the high side, Mo has the offsetting advantage of being available in foils as thin as 0.0003" and a nominal 12 inch width in continuous strips several hundred feet long. Thus there is flexibility in insulation packet design, since both the width and length (number of layers) of the assembly can be varied over wide ranges while still using only a single piece of material for the entire wrap. This avoids the possible problems involved in piecing together short sections of such ultra-thin material. A further point in favor of molybdenum is that it has been previously used in high temperature applications including MHW thermoelectric generators at about 1050°C, and vacuum furnaces operated at 1550°C. This latter application used the ZrO_2 particle separator, while the former used silica fiber cloth separators.

The final design of the multifoil packet is discussed in detail in the SIG Final Report, (TES-33009-46). Three packets of roughly similar design are used on each generator. They consist of 60 layers of 0.0003 in. Mo foil electrostatically sprayed with <0.05 μm ZrO_2 powder to a surface density of 0.06 mg/cm^2. They are given structural support by separate heavier sleeves (0.003 inch Mo on the hot side and 0.010" Ti on the cold side.) They were positioned inside the generator by three rectangular Ti tabs EB welded to the outer Ti can. These were attached to the thermoelectric modules by locating pins which engaged a spring and piston shock mounting inside the tabs (Figure 12). The overall dimensions of the Multifoil cylinders was approximately 8 inches ID by 3 inches high. The Mo foils assumed an average spacing of 0.05 inches. One complete layer of zirconium 0.007" thick was located inside the molybdenum support can as an oxygen and water getter and another layer of zirconium 0.004" thick was located twelve layers in from the titanium support can as a hydrogen getter. The Mo 0.0003" foil was perforated with six random 1/4" holes per layer to facilitate transport of the outgassing species to the getters.

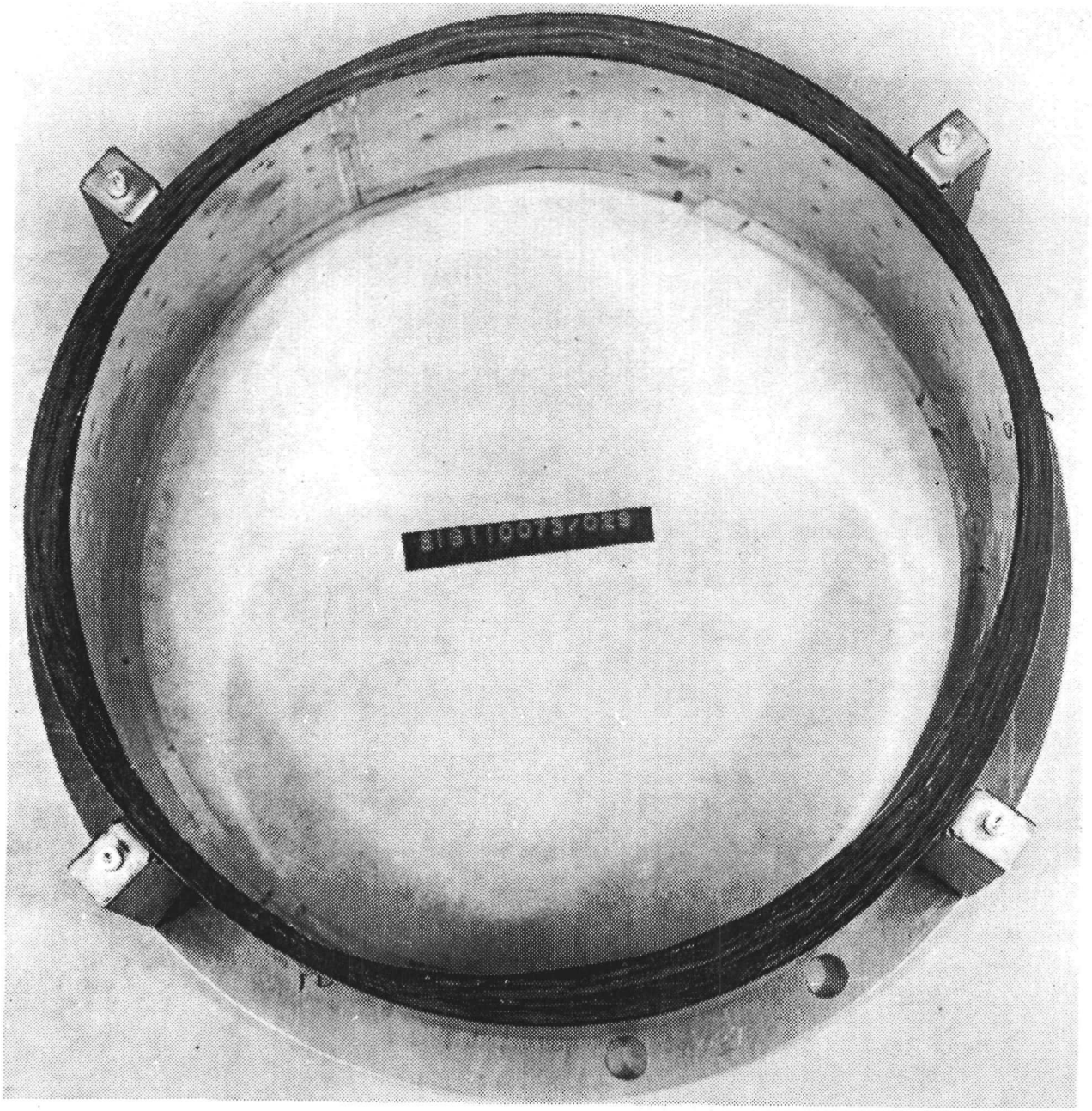

Figure 12. SIG Multifoil Insulation

Because of its very low effective thermal conductance, accurate measurements are difficult to make on Multifoil insulation, especially when the aspect ratio is as unusual as it is in this case. Therefore a series of experiments was designed to measure the effective conductivity of the base material, the effect of the perforations on thermal conductivity, the relative size of the edge losses where the multifoil contacted the fiberfrax, and the temperature distribution within the stack (to aid in locating the H_2 getter at the proper temperature).

Some reservations were expressed as to the tenacity of the ZrO_2 particles on the Mo surface during the vibration loads at launch. So a separate test was designed to check this effect and also the ability of the foil package to resist "telescoping" under vibration induced loads.

4.2 Test Results

All of the test specimens were fabricated at TECO, Waltham, Massachusetts. All heat flux measurements were also made there. The vibration test fixture was designed and built by Teledyne Energy Systems and the vibration tests were conducted at the Naval Surface Weapons Center facility in Silver Spring, Md.

4.2.1 Vibration Test

A test specimen was fabricated consisting of 30 layers of 6" high foil wrapped on an 8" ID (Figure 13). It was made this high to help the accuracy of the heat flux measurements. The aspect ratio of the SIG generator components is too unfavorable for such tests to be meaningful, especially with the small changes expected from possible mechanical changes during vibration. The stack thickness was reduced to 30 layers so as to maintain the same mass loading on the wire ties.

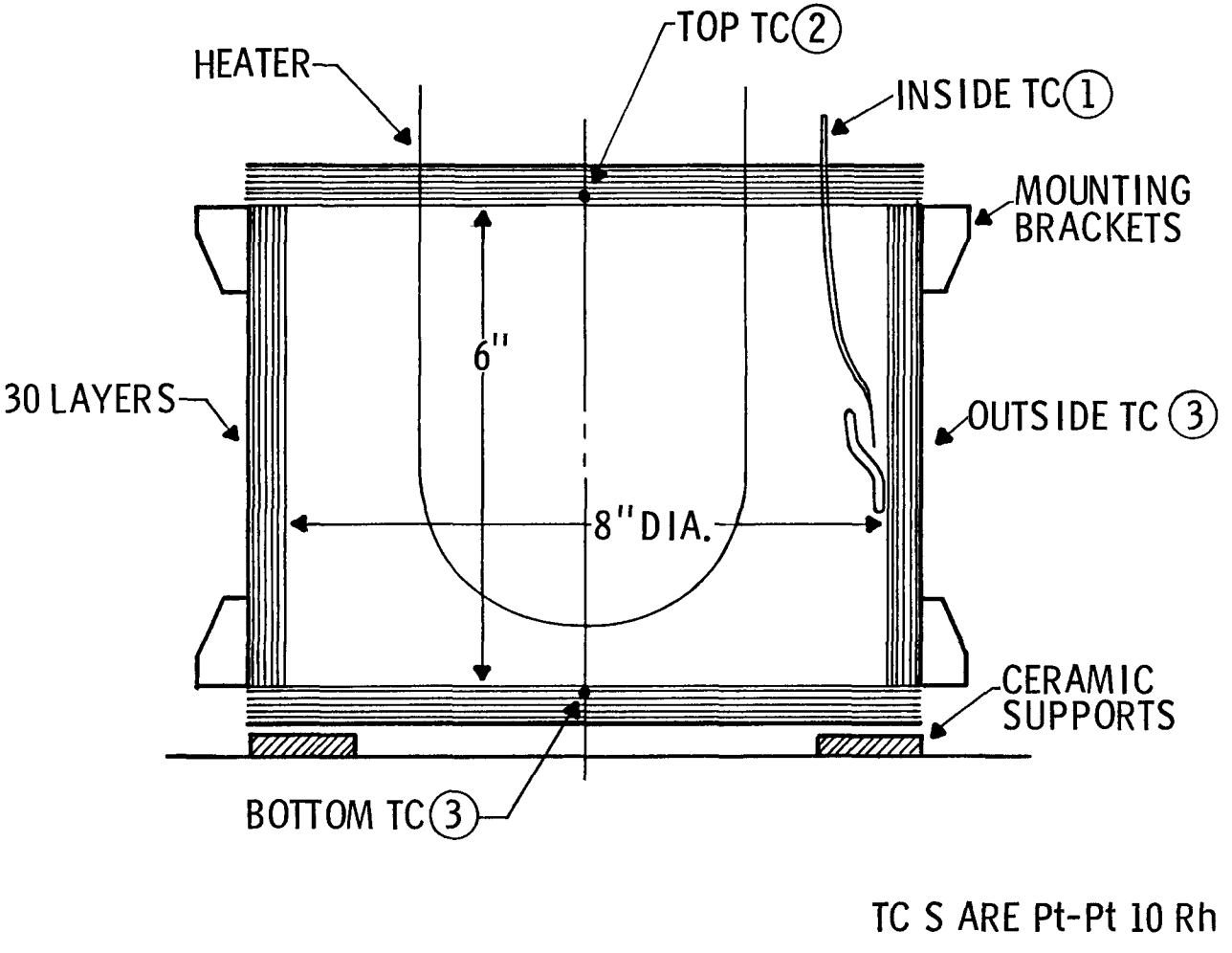

Figure 13. Test Arrangement Vibration Test Sample

The complete vibration effect evaluation consisted of the following:

1. Weigh the cylinder assembly.
2. Heat flux test 990/250°C
3. Lateral excitation (radially)
   a. Low frequency random vibration, 40 sec
   b. Qualification level random, 6 min.
4. Longitudinal excitation (axially)
   a. Low frequency random, 20 sec
   b. Qualification level random, 3 min.
   c. Sinusoidal 20-2,000 Hz range at 1g (peak) 5 min.
   d. Sinusoidal 2000-20 Hz range at 1g (peak) 5 min.
5. Lateral excitation (radially)
   a. Sinusoidal resonance search 20-2000 Hz at 1g (peak) 5 min.
   b. Sinusoidal resonance search 2000-20 Hz at 1g (peak) 5 min.
6. Reweigh cylinder assembly
7. Heat flux test 990/250°C

The multifoil sleeve assembly was mounted to the test fixture by means of rigid tabs rather than through the spring and piston shock mountings used in the generator design. Also, there was no fiberfrax against the foil edges. Thus this test was conservative in design. After the vibration test only a very slight trace of ZrO_2 particles were found on the test fixture beneath the ring, showing that that electrostatic potential between the metal and the micron sized particles was indeed substantially greater than the gravitational forces applied to the particles during vibration.

In only one section of the cylinder, the foil was found to have sagged 0.040" below the outer titanium can (Figure 14). This indicates that the six wire ties are sufficient to prevent telescoping of the assembly.

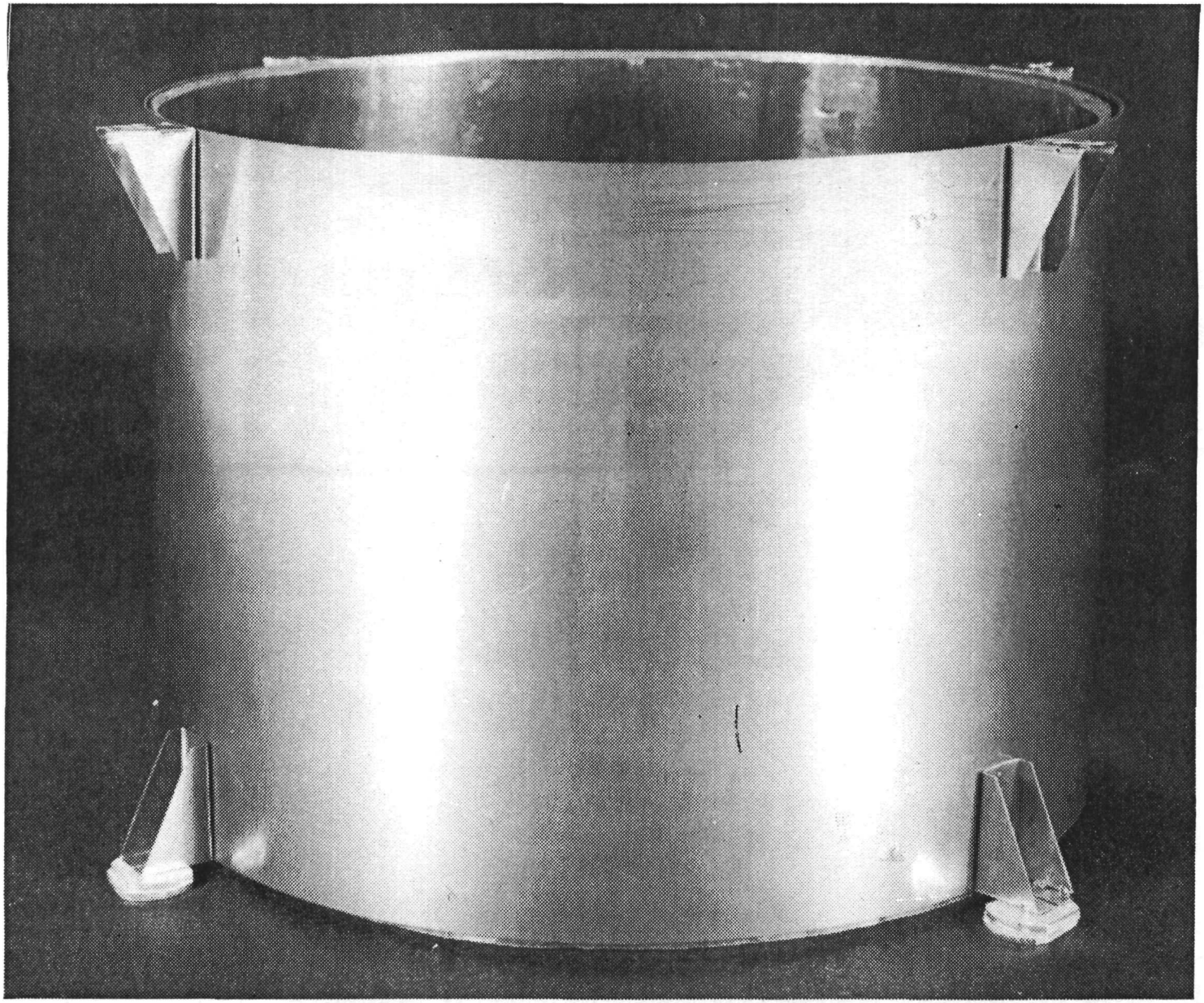

Figure 14. Multifoil Sample After Vibration Test

As was expected from the visual observation of the test fixture, there was no detectable weight change of the assembly (i.e., < 1 mg). The post vibration heat loss was 277 watts, compared to 309 watts before the vibration test. These numbers include edge losses and are well within experimental error of each other.

The vibration test results are reported in detail in SIG-EPM-1628, dated November 28, 1978.

4.2.2 Edge Effects Tests

Since multifoil insulations in vacuum environments are such efficient thermal insulators, any parasitic heat losses will account for a substantial portion of the overall bypass heat flux. It is therefore important that such losses be characterized and factored into design calculations. A major factor in the very squat aspect ratio of the SIG design is the edge loss. Open gaps at the foil/module interface would result in large radiation heat transfer losses, while plugging these gaps with fibrous insulation materials will lead to noticeable solid conduction losses.

In order to evaluate such effects, a series of tests was performed using straight foil contact at the edges and using Fiberfrax 660 Hi-Fi Paper to fill the gaps between the covers and the edtes of the multifoil cannisters. The test set-up is shown schematically in Figure 15

The test cylinders consisted of 60 layers of 0.0003 inch thick Mo foil at an average separation of 0.005 inches. The foil was electrostatically coated with $\sim$1 μm ZrO_2 particles to a surface density of 0.06 mg/cm^2. Three different cylinder heights (2, 4, and 6 inches) were used to obtain differential heat flux data on the multifoil cannister. All of the cannisters were 8 inches in diameter.

An extremely large amount of scatter was observed when these tests were first run. Much of the problem was considered to be due to the use of an unshielded heater filament and the very low aspect ratio which greatly exaggerates any edge loss phenomena. There

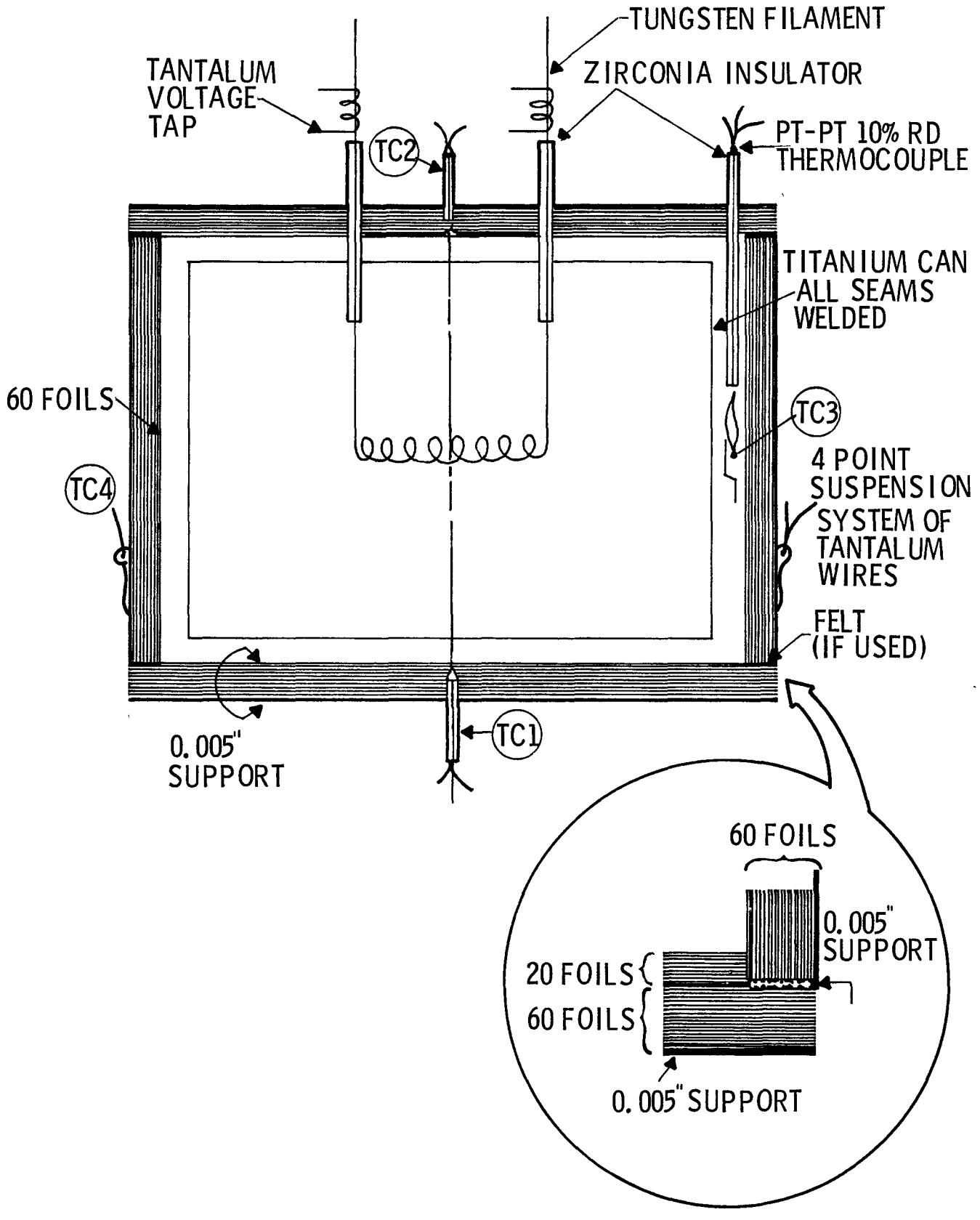

Figure 15. Test Arrangement Edge Effect Samples

was also some additional loss contributed by uneven compression of the multifoil base. The tests were repeated using a light-tight titanium can around the heater to ensure that any radiation streaming through the edges would be from a 990°C source, rather than from a 1500°C filament. The weight of the cylinder was also supported by tantalum wires to relieve the compression problem on the base foils. This led to somewhat more consistent results.

The test results are reported in Table 8 for this second set of experiments. Very wide scatter was obtained with the unpacked edges to such an extent that the direct radiation losses through the openings in the 2" high cylinder overshadowed the heat flux through the multifoil itself. This is partially due to the previously mentioned poor aspect ratio (1:0.25) and partly attributable to uncertainties in the heat losses through the 5 thermocouples and heater leads and their insulators. The aspect ratios of the 4 and 6 inch cylinders (1:0.5 and 1:0.75) were only slightly better.

The data from the 4 inch and 6 inch cylinders was used to estimate the flux through the multifoil at a 990°C source temperature. The value of 0.035 w/cm^2 is within experimental error of the 0.031 w/cm^2 predicted from earlier studies performed by TECO on Ni foils. When the data are adjusted for conduction losses through the five feedthroughs, the edge losses for the Fiberfrax packed samples are indicated to be between 0.2 w/cm and 0.3 w/cm. Well designed multifoil joints with 3 or 4 steps have been shown to have edge losses of approximately 0.1 w/cm.

4.2.3 Perforation Tests

The Multifoil cylinders in the SIG system are perforated to allow more efficient gettering of outgassing products at both the high temperature and low temperature zirconium getters. The magnitude of the effect of such perforations was checked experimentally by measuring the heat flux through a 6 inch high 60 layer cylinder with 30 randomly spaced 0.25 inch holes per layer. The results of this test were compared with those of the 6 inch high sample of the edge effect tests.

TABLE 8

Edge Loss Test Results

	P	T_H	T_C	ϕ w/cm^2
6"	126.11 w	990	158	.050
6" Felt	111.54	990	122	.035
4"	109.81 w	990	125	.050
4" Felt	100.06	990	98	.035
2"	127.08 w	990	235	(higher losses than larger samples)
2" Felt	106.80	990	154	.054

These tests were run with the unshielded heater configuration only. The results indicated that one could get a 6-13% increase in the SIG configuration Multifoil with six holes per layer. Since the normal experimental variation band on these systems is higher than this (± 20%), the tests were not repeated using the shielding cannister on the filament.

4.2.4 Thermal Profile Tests

A six inch high 60 layer cylinder was instrumented with thermocouples every five layers in an effort to obtain a good thermal profile of the Multifoil package so that the optimum location for the hydrogen getter could be established.

Tests were run both with and without the inner shielding cannister. The scatter of data was very high in both cases. The results of the shielded filament test are shown in Figure 16. The thermocouples were wrapped in at every fith layer and were insulated with zirconia felt. The TECO personnel were unable to definitely locate the cause of the extremely wide scatter. Earlier tests at TECO used only 4 to 5 thermocouples inserted into the wrappings, and yielded fairly consisten linear results. Apparently the present test was "overinstrumented". It appears likely that the insertion of twelve thermocouples with the associated ceramic felt insulation, and the additional manipulation required to complete the test set-up, probably caused severe distortion at various points in the stack and allowed some localized hot spots to be caused by direct conduction.

It is recommended that any future tests of this type should use a minimal number of thermocouples placed at approximately the depth indicated by calculations to give the required getter temperature.

4.3 Discussion

Many attempts have been made in the past to develop good analytical models for the thermal conductance of multilayer insulation systems. However, because of the large number

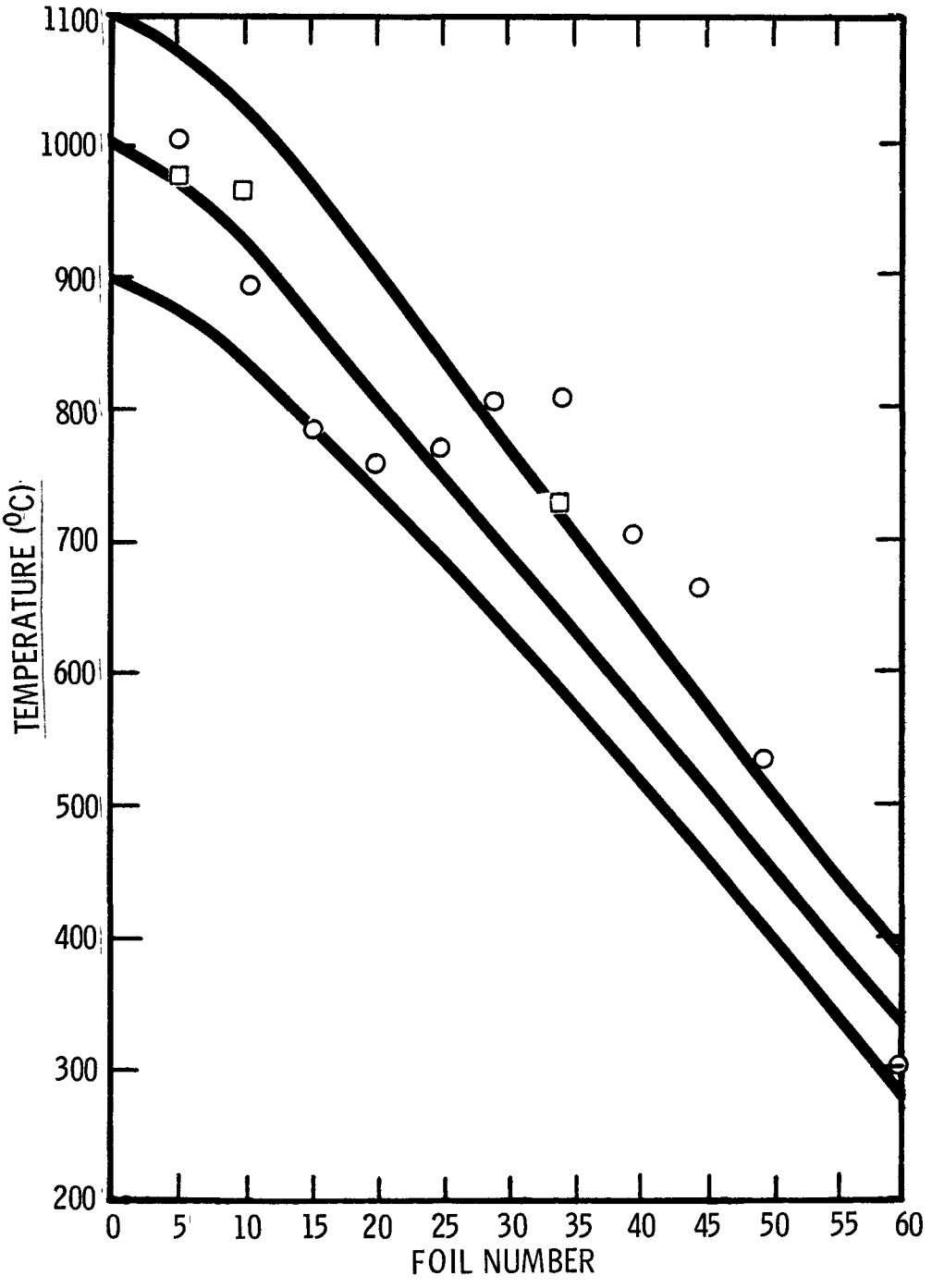

Figure 16. Measured Temperature Distribution Through Cylindrical Foils (Ni)

of uncontrollable variables in such systems they all revert to determining empirical constants which are more or less related to the emissivity and effective solid conductivity of the insulation.

Such an expression was developed by TECO for nickel multifoil packets of varying geometries and temperature ranges. It was later shown to be applicable to other high temperature Multifoil systems using tungsten, tantalum, and molybdenum to predict the heat flux within about 20%.

$$\phi = \frac{1.06 \times 10^{-12} \ (T^4 - 81 \times 10^8)}{0.778\ N + (1.11 \times 10^{-2})\ N^2}$$

where:

ϕ = heat flux perpendicular to the foils (watts/cm^2)

T = heat source temperature, K

N = number of foils.

From the numerator constant the effective emissivity of the Ni-ZrO_2 combination is estimated at 0.32 which is in agreement with reported values determined for sand blasted nickel foil. Thus it would seem that the ZrO_2 particles cause the surface of the nickel to be optically roughened, while not contributing materially to the solid conduction. This latter effect is presumably accounted for by the N^2 term in the denominator.

The tenuous bonding of the zirconia particle spacer to the foil layers is essential to the insulation characteristics of Multi-Foil. Such a bond has a high thermal contact resistance which minimizes conduction heat losses through the foil assembly.

The electrostatic force which holds the particles to the foil surface is due to the contact potential arising from the differing work functions of the materials. The work function of a material is the difference between the Fermi level and the electrostatic potential at the surface. Typically, the work function of most materials varies between 3.5 and 5.5 electron volts.

The electrostatic force thus applied to small particles can be rather large compared to the gravitational force on such particles. Figure 17 indicates how the electrostatic forces can easily hold micron size particles on surfaces even in the presence of high vibrational g-loads. (Ref. 10).

The scanning electron microscope picture of a 0.01 mm^2 area of the Mo foil used in our tests shown in Figure 18 contains 304 particles. Of these 283 or 93% are 3 μm or under. As can be seen in Figure 17 the electrostatic force between the foil and particle is of the order of 100 times the force of gravity. Similarly, 99% of the particles are 5 μm or under. This would still indicate an electrostatic force about 30 times the force of gravity. Thus if the assumptions are correct we would expect less than one per cent of the particles to be dislodged during vibration to levels of ten to twenty G's.

This was qualitatively confirmed in our vibration tests where only a slight trace of powder was observed on the fixture beneath the Multifoil after the full series of tests.

TECO's previous data from tests using various coating densities indicated that a loss of oxide particles approaching 20% would be required to cause measurable heat transfer changes.

The fact that no increase in thermal conductance was observed as a result of the vibration tests also helps confirm the above model.

Since the perforations to help transport the gaseous species to the getters remove only about 0.4% of each layer and even this small fraction is distributed among six randomly spaced holes, very little effect was expected to be noticed in the thermal conductance. This was confirmed by measurements of heat flux in which the perforated and unperforated samples were within experimental error of each other for 6 holes per layer.

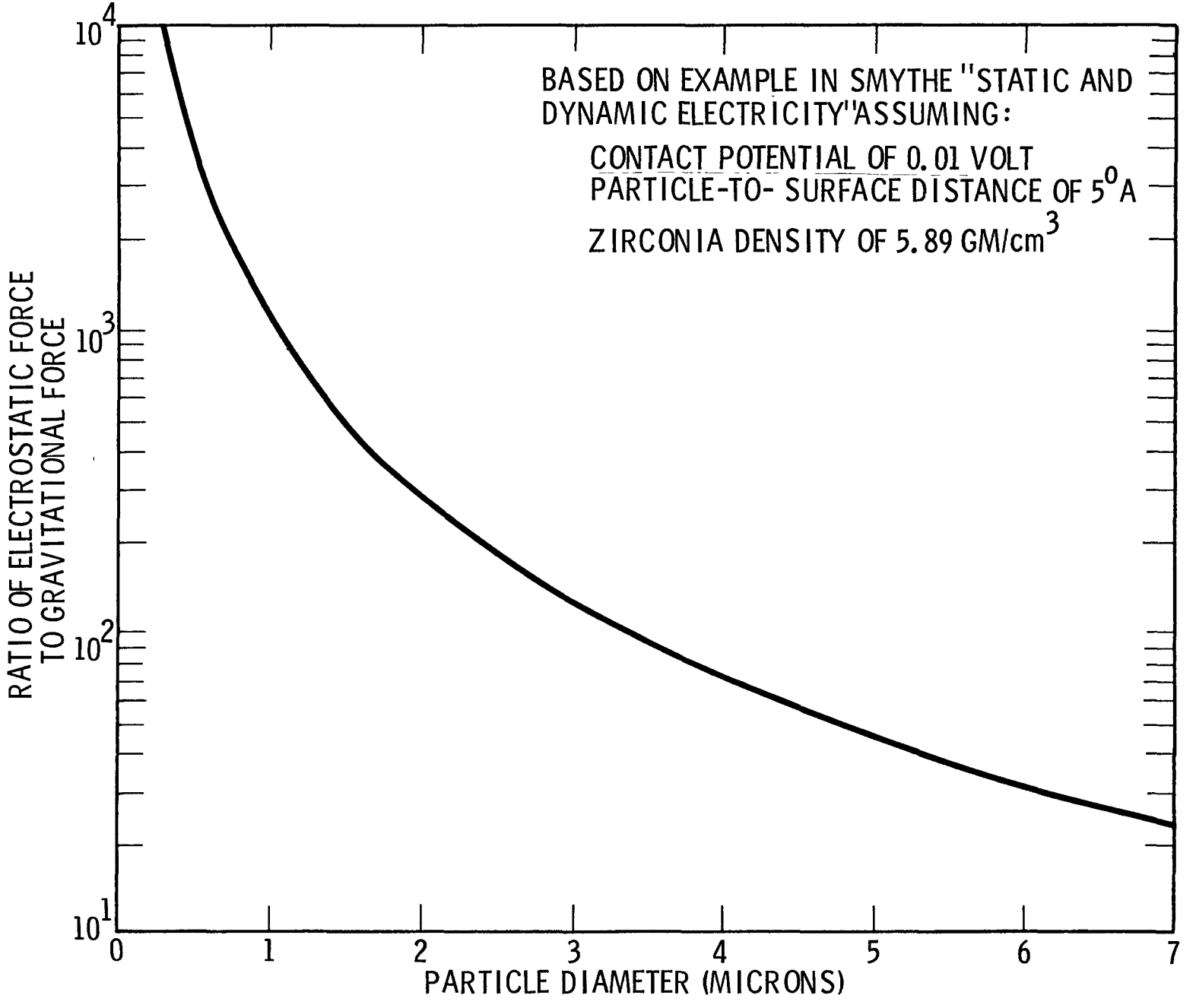

Figure 17. Ratio of Electrostatic Force to Graviational Force as a Function of Particle Diameter.

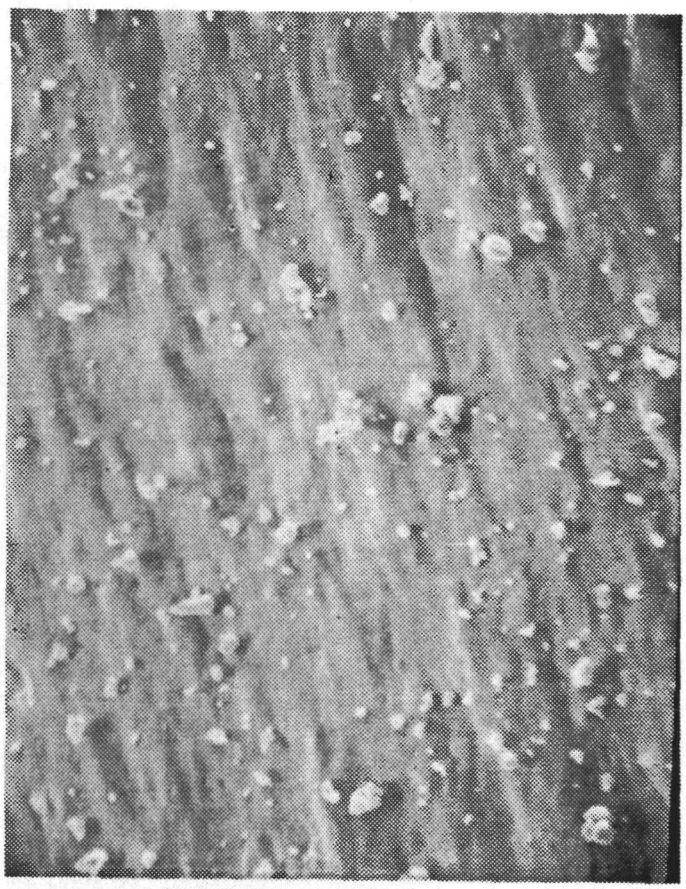

Figure 18. Scanning Electron Microscope Picture of ZrO_2 Particles on Mo (1000X)

The edge effect tests were much less conclusive due to the aspect ratio problems mentioned earlier. However, the values of 0.2 to 0.3 watts/cm are in line with earlier data which indicated 0.5 w/in. for flat joints and 0.1 w/in. for three or four step joints in all multifoil systems. The Fiberfrax paper would certainly be expected to cut down the radiation losses significantly, but nearly all fibrous insulations are known to have a higher thermal conductivity than foils in vacuum.

In summary, then, these tests have demonstrated that the ZrO_2 coated molybdenum Multifoil system can be made to perform under the launch and flight conditions specified for SIG/Galileo. An analytical expression is available for use in predicting the thermal performance of the multifoil itself to within ± 20%. However, the edge losses are more difficult to pin down, especially in this hybrid system where the uniformity and continuity of the Fiberfrax packing are so important to the overall result. The large relative contribution from the fibre stuffed edges point to the necessity of very good design, manufacturing, assembly, and quality control procedures for this type system.

For the future collection of data of this type it would be very advantageous to work with much higher aspect ratio samples (e.g., 6:1 or better) and then to calculate the values for the actual hardware geometries.

5.0 REFERENCES

1. ASTM Standard C177-76, American Society for Testing and Materials, Philadelphia, PA, 1978

2. Teledyne Energy Systems, SIG30060 "Outgassing Procedure for Carbon, Graphite and Boron Nitride Materials", and SIG30064 "Bakeout and Outgassing Procedure for Oxide Type Thermal Insulation and Electrical Insulation Materials."

3. a. Johns-Manville, P.O. Box 5108, Denver, Colorado 80217

   b. Micropore Insulation Ltd., Stourport Road, Kidderminster, Worcestershire, England

   c. Oak Ridge National Laboratories, Metals and Ceramics Division, Oak Ridge, Tennessee, 37830

   d. Zircar Products Inc., 110 North Main St., Florida, N.Y. 10921

   e. Cotronics Corporation, 37 West 39th St., New York, N.Y. 10018

   f. Carborundum Company, Refractories and Electronics Division, P.O. Box 339, Niagara Falls, N.Y. 14302

   g. Glasrock Products, Inc., 2210 Marietta Blvd., N.W., Atlanta, GA 30318.

   h. Chemotronics International Incorporated, 2231 Platt Road, Ann Arbor, Michigan 48104.

4. R.P. Type, "Thermal Conductivity of Min-K 2000 Thermal Insulation in Different Environments to High Temperatures", 9th Conference on Thermal Conductivity, Iowa State Univ., Ames, Iowa, Oct. 1969.

5. T.G. Godfrey, D.L. McElroy, and Z.L. Ardary "Thermal Conductivity of Oriented Fibrous Carbon Insulation from 300 to 1300 K in Nitrogen and Argon at One Atmosphere" Nuclear Technology 22, 94-107 (1974).

6. Collins, J.O., et. al. "Develop 1800F-400F Fibrous Type Insulation for Radioisotope Power Systems, Final Report (#ALO-2661-12), Contract AT(29-2)-2661, Johns-Manville Research and Engineering Center, Manville, N.J., Feb. 1969.

7. Skrabek, E.A., "Ammendment to Test Plan for Insulation Load Bearing Experiment" LCHPG-EAS-508A, Aug. 24, 1976, Teledyne Energy Systems.

8. F. Notaro and W.E., Grunert, "Multilayer Vacuum Insulations in High Temperature Systems, Proceedings 5th IECEC, Las Vegas, Nevada, Sept. 1970.

9. "Application of MULTI-GOIL Insulation to the Brayton Isotope Power System and Conceptual Design of MULTI-FOIL Insulation for the Flight System" Thermo-Electron Report No. 4209-100-76, June 11, 1976, Waltham, Mass.

10. Dushmann S. and Lafferty, J.M., "Scientific Foundations of Vacuum Technique" 2nd Ed., Wiley-Interscience, New York, N.Y. 1962.

11. Smythe, W.R., "Static and Dynamic Electricity" 3rd Ed., McGraw-Hill Book Co., New York, N.Y. 1968.